

MOTION VERIFIED RED STARS (MoVeRS): A CATALOG OF PROPER MOTION SELECTED LOW-MASS STARS FROM *WISE*, SDSS, AND 2MASSCHRISTOPHER A. THEISSEN¹, ANDREW A. WEST¹, AND SAURAV DHITAL²

ABSTRACT

We present a photometric catalog of 8,735,004 proper motion selected low-mass stars (KML-spectral types) within the Sloan Digital Sky Survey (SDSS) footprint, from the combined SDSS Data Release 10 (DR10), Two-Micron All-Sky Survey (2MASS) Point Source Catalog (PSC), and *Wide-field Infrared Survey Explorer* (*WISE*) AllWISE catalog. Stars were selected using $r - i$, $i - z$, $r - z$, $z - J$, and $z - W1$ colors, and SDSS, *WISE*, and 2MASS astrometry was combined to compute proper motions. The resulting 3,518,150 stars were augmented with proper motions for 5,216,854 earlier type stars from the combined SDSS and United States Naval Observatory B1.0 catalog (USNO-B). We used SDSS+USNO-B proper motions to determine the best criteria for selecting a clean sample of stars. Only stars whose proper motions were greater than their 2σ uncertainty were included. Our Motion Verified Red Stars (MoVeRS) catalog is available through SDSS CasJobs and VizieR.

Keywords: catalogs — infrared: stars — proper motions — stars: low-mass — stars: kinematics and dynamics — stars: late-type

1. INTRODUCTION

Over the past century, photometric surveys—both digital and photographic—have played an important role in many facets of astronomy. One of the largest limitations to these surveys has been object classification for point sources that have similar colors and morphologies (e.g., M giants, M dwarfs, QSOs, and distant luminous red galaxies). One method for separating nearby stellar populations from more distant objects is measuring tangential motion on the sky, or *proper motion*. Proper motions are also important for distinguishing and investigating kinematically distinct populations within our Galaxy (e.g., moving groups, disk and halo stars, etc.).

A number of large, all-sky catalogs of stellar positions and proper motions now exist. The United States Naval Observatory (USNO) has had a long history of tracking astrophysical objects, starting with their first published catalog UJ1.0 (Monet et al. 1994), and subsequently replaced by USNO-A1.0 (Monet 1996), USNO-A2.0 (Monet 1998), and ultimately USNO-B1.0 (Monet et al. 2003, hereafter USNO-B). These catalogs are the result of the Precision Measuring Machine at the USNO Flagstaff Station, undertaking a photometric survey over ~ 50 years on Schmidt plates. USNO-B culminated in a catalog containing the positions, proper motions, and magnitudes for over a billion objects. However, the proper motions and positions in USNO-B are relative, not absolute, making it difficult to compare observations with later epoch observations on a well-defined system (e.g., Röser et al. 2008, 2010). Other proper motion catalogs of note include (but are not limited to): the SUPERBLINK catalog of northern stars with large proper motions (Lépine & Shara 2005, hereafter LSPM), the Positions and Proper Motions catalog (PPM, PPMX, PP-

MXL; Röser & Bastian 1993; Röser et al. 2008, 2010), and catalogs calibrated with the Sloan Digital Sky Survey (SDSS; York et al. 2000) and USNO-B (Munn et al. 2004; Gould & Kollmeier 2004) surveys.

One of the newest surveys from the USNO is the CCD Astrograph Catalog (UCAC; Zacharias et al. 2000), now in its 4th (and final) data release (UCAC4; Zacharias et al. 2013). While UCAC4 does not contain as many objects as USNO-B1.0 ($\sim 10^8$ objects), and has a shorter time baseline (~ 6 yrs), it is approximately five times more precise (Zacharias et al. 2000) due to the use of CCDs instead of photographic plates. UCAC is also in an absolute reference frame, the International Coordinate Reference System (ICRS). The newest undertaking (started in April 2012) by the USNO is the USNO Robotic Astrometric Telescope (URAT), currently in its initial data release with (URAT1; Zacharias et al. 2015). This catalog is expected to achieve precision astrometric measurements (~ 10 mas) for 500 million sources, but will be relatively shallow in comparison to other surveys ($R \approx 18$; Zacharias & Gaume 2011), and it will be many years before the deepest all-sky data release (northern and southern hemisphere) is available.

The best example to date of high-precision space based astrometry is the survey performed by the *Hipparcos* satellite (ESA 1997), making precise astrometric measurements (< 10 mas) for millions of stars. The current realization of *Hipparcos* data is the Tycho-2 catalog (Høg et al. 2000), containing astrometric information for approximately 2.5 million stars. Prior to Tycho-2, the *Hipparcos* catalog (Perryman et al. 1997), containing extremely high precision astrometric measurements for 118,218 stars, defined the ICRS at optical wavelengths. The ICRS is the standard reference frame that modern surveys (e.g., SDSS, and the future Large Synoptic Survey Telescope or LSST; Ivezić et al. 2008) use to calibrate their astrometry, since the majority of these surveys are tied to either Tycho-2 or UCAC.

Although many proper motion catalogs exist, they are typically tied to surveys that are biased towards the blue

Electronic address: ctheisse@bu.edu

¹ Department of Astronomy, Boston University, 725 Commonwealth Avenue, Boston, MA 02215, USA² Department of Physical Sciences, Embry-Riddle Aeronautical University, 600 South Clyde Morris Blvd., Daytona Beach, FL 32114, USA

end of the spectrum (e.g., USNO-B). This makes most current proper motion catalogs severely incomplete at the lowest-mass end of the main-sequence, save a few smaller catalogs (e.g., Lépine & Shara 2005; Deacon & Hambly 2007; Faherty et al. 2009). It is only in recent years that an all-sky infrared point-source catalog with enough astrometric precision to build a more complete proper motion catalog for the reddest point sources has become available. Combining observations from all-sky and large area surveys taken over the past two decades will allow us to compute reliable proper motions for the lowest-mass stars.

The past two decades have seen the emergence of three of the most important astronomical surveys for studies of low-mass stars: the Two Micron All-Sky Survey (2MASS; Skrutskie et al. 2006), SDSS, and the *Wide-field Infrared Survey Explorer* (*WISE*; Wright et al. 2010). 2MASS conducted observations between 1997 and 2001 in three near-infrared (NIR) bands (J : 1.25 μm , H : 1.65 μm , and K_s : 2.17 μm). The 2MASS point source catalog (PSC) contains over 470 million objects. SDSS conducted visible wavelength observations starting in 2000, with some observations as recent as the last five years. SDSS observed the sky in five visible wavelength bands (*ugriz*), and Data Release 10 (DR10; Ahn et al. 2014) contains approximately 260 million point sources. *WISE* began observing the entire sky in 4 mid-infrared bands (3.4, 4.6, 12, and 22 μm) starting in 2010. A second post-cryogenic mission (NEOWISE; Mainzer et al. 2011) was carried out at the end of 2010 using the two shortest bands, and surveying the entire sky over the course of a year. The AllWISE catalog combines both *WISE* missions to create a catalog with enhanced photometric sensitivity and accuracy, and improved astrometric precision above each individual mission’s data products. The AllWISE catalog contains over 747 million objects. Combining these three surveys provides a time baseline of ~ 10 years.

The ubiquity of M dwarfs throughout the Galaxy ($\sim 70\%$ of the total stellar population; Bochanski et al. 2010), coupled with the fact that M dwarfs have main-sequence lifetimes longer than the current age of the Universe ($\sim 10^{12}$ yrs; Laughlin et al. 1997), make M dwarfs important laboratories for studying numerous aspects of astronomy (e.g., Galactic and stellar evolution, kinematics, etc.). Recent results have also suggested that M dwarfs have a strong penchant for building terrestrial planets (e.g., Dressing & Charbonneau 2013, 2015). This affinity for creating terrestrial planets, coupled with the relative ease for finding terrestrial planets around M dwarfs (due to their size ratios and small orbital distances), make M dwarfs important hosts for studying Earth-sized planets and habitability throughout the Galaxy.

Many large catalogs of M dwarfs (dMs) currently exist, including the Palomar/Michigan State University (PMSU; Reid et al. 1995; Hawley et al. 1996) survey (~ 2400 spectroscopic dMs), and the SDSS Data Release 7 (DR7; Abazajian et al. 2009) spectroscopic catalog (70,841 spectroscopic dMs; West et al. 2011). However, such catalogs make up only a small fraction of the millions of photometric dMs contained within SDSS. For example, Bochanski et al. (2010) used SDSS DR7 to retrieve ~ 15 million photometrically selected, but not

proper motion verified, dMs to investigate the mass and luminosity functions of the Galactic disk. While most of the red point sources in SDSS are M dwarfs rather than giants or red galaxies for the color and magnitude range chosen by Bochanski et al. (2010), proper motions can help to select *bona-fide* low-mass stars.

Gaia (Perryman et al. 2001) is currently conducting the largest astrometric survey to date. *Gaia* is a magnitude limited survey, the limits of which are shallower ($r \leq 20$; Ivezić et al. 2012) than the combined *WISE*+SDSS limits ($r \leq 22.2$), making *Gaia* incomplete for the faintest and lowest-mass (reddest) stars. Approximately 60% of the stars in the combined photometric dataset of *WISE*, SDSS, and 2MASS have $r \geq 20$, making the majority of low-mass stellar candidates beyond the reach of *Gaia* (for relative point-source densities at different r magnitudes see Figure 6 of Bochanski et al. 2010).

To make use of a larger photometric sample of dMs within SDSS, we combine *WISE*, SDSS, and 2MASS observations to compute proper motions over ~ 10 year baselines for photometrically selected objects with dM colors. After a color cut and selection of reliable proper motions, we are left with a sample of 8,735,004 stars. In Section 2, we outline our methods for computing proper motions and errors. We also estimate the intrinsic uncertainty within our catalog using SDSS selected quasars. In Section 3, we discuss the selection criteria used to build our photometric dM sample, and address contamination (Section 3.4). In Section 4 we assess the reliability of our catalog. We augment our derived proper motions with measurements from SDSS+USNO-B in Section 5. In Section 6, we discuss the properties of our Motion Verified Red Stars (MoVeRS) catalog and how to query it. We describe preliminary science results that can be achieved with this catalog in Section 7. Our summary follows in Section 8.

2. METHODS: COMBINING *WISE*, SDSS, AND 2MASS

2.1. Astrometric Algorithms

SDSS was originally calibrated against UCAC and Tycho-2 (Pier et al. 2003), but as of its seventh data release (DR7) was calibrated against UCAC2 and an internal UCAC release known as “r14³.” This recalibration reduced systematic errors from ~ 75 mas (Tycho-2) and ~ 45 mas (UCAC) to less than 20 mas⁴. SDSS is also on the ICRS since the Tycho-2 catalog is based upon *Hipparcos* astrometry, which defines the ICRS at visible wavelengths. All SDSS astrometric calibrations for this study were performed in the r -band.

We noticed that SDSS positional errors (RAERR, DECERR) in all SDSS Data Releases more recent than DR7 are pixel-centroiding errors rather than absolute astrometric errors (B. A. Weaver, personal communication). To compute absolute astrometric errors, we found the total error (centroiding plus calibration) in great circle coordinates using the following equations,

$$\sigma_{\mu} = \sqrt{(\text{ROWCERR} \times 0.3961)^2 + \text{MUERR}^2} \quad (1)$$

³ <https://www.sdss3.org/dr10/algorithms/astrometry.php>

⁴ <http://classic.sdss.org/dr7/algorithms/astrometry.html>

and

$$\sigma_\nu = \sqrt{(\text{COLCERR} \times 0.3961)^2 + \text{NUERR}^2}, \quad (2)$$

where ROWCERR and COLCERR are the row center and column enter position errors in r -band coordinates, respectively, and are found in the SDSS CasJobs “PHOTOOBJ” table. The fields MUERR and NUERR are the astrometric errors in Great Circle coordinates (μ and ν) for the r -band, and are found in the “Field” table. The factor of 0.3961 is the SDSS pixel scale (arcsec pix⁻¹). Next, using the above total errors in Great Circle coordinates, we converted to α and δ through the following equations,

$$s = -\sin(\text{INCL}) \sin(\text{NU}) \sin(\text{MU} - \text{NODE}) + \cos(\text{INCL}) \cos(\text{NU}), \quad (3)$$

$$c = -\sin(\text{INCL}) \cos(\text{MU} - \text{NODE}), \quad (4)$$

$$\sigma_{\alpha\text{SDSS}} = \sqrt{(c \cdot \sigma_\mu)^2 + (s \cdot \sigma_\nu)^2}, \quad (5)$$

and

$$\sigma_{\delta\text{SDSS}} = \sqrt{(s \cdot \sigma_\mu)^2 + (c \cdot \sigma_\nu)^2}, \quad (6)$$

where MU, NU, NODE, and INCL refer to fields in the SDSS CasJobs “Frame” table. MU and NU refer to the Great Circle coordinates of the frame center, and INCL and NODE are the inclination and right ascension of the ascending node of the scan Great Circle with respect to the J2000 celestial equator⁵.

The 2MASS PSC uses the Tycho-2 catalog to reconstruct its coordinates in the ICRS⁶, with accuracies between 70–120 mas. 2MASS astrometric errors are reported as an error ellipse with the entries ERR_MAJ (σ_{MAJ}), ERR_MIN (σ_{MIN}), and ERR_ANG (σ_θ). These were converted to σ_α and σ_δ components using the following equations,

$$\sigma_{\alpha 2\text{MASS}} = \sqrt{(\sigma_{\text{MAJ}} \cdot \sin \sigma_\theta)^2 + (\sigma_{\text{MIN}} \cdot \cos \sigma_\theta)^2} \quad (7)$$

and

$$\sigma_{\delta 2\text{MASS}} = \sqrt{(\sigma_{\text{MAJ}} \cdot \cos \sigma_\theta)^2 + (\sigma_{\text{MIN}} \cdot \sin \sigma_\theta)^2}. \quad (8)$$

Relative astrometric calculations for 2MASS and *WISE* are computed on the unit sphere, and therefore the α component of the astrometric uncertainties already accounts for the $\cos \delta$ term (Vandana Desai, personal communication).

WISE is tied to the ICRS through 2MASS. However, to address possible systematic proper motion shifts between the two catalogs due to their different epochs, the *WISE* pipeline used proper motion data from UCAC4 to readjust 2MASS positions before they were used as reference stars⁷. Estimated errors for the source catalog are < 100 mas. *WISE* astrometric errors are denoted by the entries SIGRA (σ_{SIGRA}) and SIGDEC (σ_{SIGDEC}).

⁵ <https://www.sdss3.org/dr10/algorithms/astrometry.php>
⁶ http://www.ipac.caltech.edu/2mass/releases/allsky/doc/sec2_2.html
⁷ http://wise2.ipac.caltech.edu/docs/release/allwise/expsup/sec2_5.html

For sources with only two observation epochs, the uncertainties for each proper motion component are given as

$$\sigma_{\mu_\alpha}^2 = \left(\frac{\cos \bar{\delta}}{\Delta_t} \right)^2 \left[\sigma_{\alpha_1}^2 + \sigma_{\alpha_2}^2 + \left(\frac{\Delta_\alpha}{\Delta_t} \right)^2 (\sigma_{t_1}^2 + \sigma_{t_2}^2) + \sigma_{\bar{\delta}}^2 \tan^2 \bar{\delta} \right] \quad (9)$$

and

$$\sigma_{\mu_\delta}^2 = \Delta_t^{-2} \left[\sigma_{\delta_1}^2 + \sigma_{\delta_2}^2 + \left(\frac{\Delta_\delta}{\Delta_t} \right)^2 (\sigma_{t_1}^2 + \sigma_{t_2}^2) \right], \quad (10)$$

where $\Delta_\alpha = \alpha_2 - \alpha_1$, $\Delta_\delta = \delta_2 - \delta_1$, $\Delta_t = t_2 - t_1$, $\bar{\delta}$ is the weighted-mean declination, and $\sigma_{\bar{\delta}}$ is the error in the weighted mean declination. Here, α , δ and t refer to the position and time, with “1” being the first epoch and “2” the second epoch. The final term in σ_{μ_α} is orders of magnitude smaller than 1 mas yr⁻¹ and is therefore negligible. Proper motion errors for the α component are in proper units (i.e. $\Delta_\alpha \cdot \cos \delta$).

On average, the temporal uncertainty is much smaller than the time baseline between measurements ($\sigma_t \approx 60$ seconds for 2MASS and SDSS). The AllWISE catalog combines observations from the initial *WISE* mission and the post-cryogenic *NEOWISE* survey. We define the temporal uncertainty to be halfway between the difference of the most recent observation and the earliest observation in the *W1*-band (i.e. $\sigma_{t\text{WISE}} = [\text{W1MJD}_{\text{MAX}} - \text{W1MJD}_{\text{MIN}}]/2$). As is shown in Figure 1, this causes some observations to have temporal uncertainties between 80–200 days. For sources with time baselines of at least four years, this uncertainty is $\lesssim 1$ mas yr⁻¹. However, a small fraction of our sources have time baselines of about one year. For this reason, we do not remove the temporal uncertainty term of the proper motion error. Our motivation for using the AllWISE catalog rather than the All-Sky Release Catalog is that the AllWISE catalog has better astrometric accuracy. This is due to the inclusion of proper motions to correct 2MASS astrometric reference stars for the greater than nine year baseline between the *WISE* and 2MASS surveys.

For sources with three observational epochs (i.e. *WISE*, SDSS, and 2MASS), we computed a weighted linear fit to the positions versus time. Rather than use an linear least squares approach, which requires the uncertainty in the independent variable (in this case time), to be negligible, we chose to invoke an Orthogonal Distance Regression (Boggs & Rogers 1990) method to calculate proper motions in each component (α , δ) separately. This allows us to take into account the sometimes significant temporal uncertainties on *WISE* observations.

2.2. Precision: Measuring the Motions of SDSS Quasars

To investigate the intrinsic error in the proper motions for each survey, we required stable objects on the sky with essentially zero tangential motion. Quasars make ideal calibrators due to their high luminosities and extragalactic distances. We used the DR10 SDSS quasar catalog (Pâris et al. 2014), which contains 166,583 spectroscopically confirmed quasars. Using this catalog, we

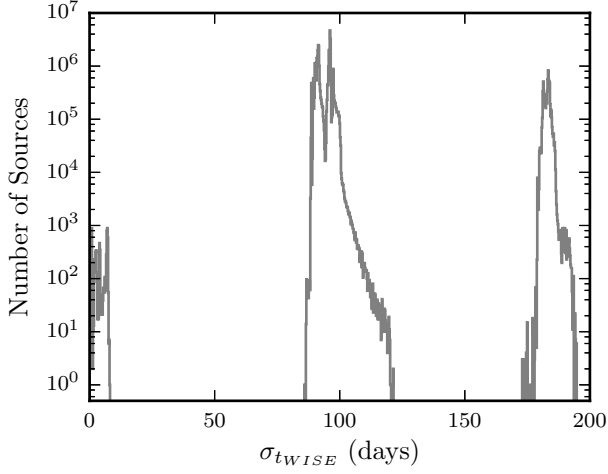


Figure 1. *WISE* temporal uncertainties for our sources. The large uncertainties are due to the AllWISE catalog being a composite of *WISE* and *NEOWISE* observations. This temporal uncertainty will account for $< 1 \text{ mas yr}^{-1}$ in our astrometric solution for stars with baselines > 4 years, however, we account for it since a small subset of our observations have baselines of ~ 1 year.

Table 1
Limits for *WISE*, SDSS, and 2MASS

Survey	Band	Limiting Magnitude (mags)	Limiting Flux ($\text{ergs s}^{-1} \text{ cm}^{-2} \text{ \AA}^{-1}$)
SDSS	<i>r</i>	22.2 (AB)	$\sim 4 \times 10^{-18}$
SDSS	<i>i</i>	21.3 (AB)	$\sim 6 \times 10^{-18}$
SDSS	<i>z</i>	20.5 (AB)	$\sim 8 \times 10^{-18}$
2MASS	<i>J</i>	15.8 (Vega)	$\sim 2 \times 10^{-17}$
2MASS	<i>H</i>	15.1 (Vega)	$\sim 4 \times 10^{-17}$
2MASS	<i>K_s</i>	14.1 (Vega)	$\sim 8 \times 10^{-17}$
<i>WISE</i>	<i>W1</i>	17.1 (Vega)	$\sim 10^{-18}$

cross-matched to both the 2MASS PSC and *WISE* AllWISE source catalog. Matching was done using search radii in steps of $0.5''$ out to $4''$, the results of which are shown in Figure 2. The number of unique matches reaches a maximum at $0.5''$ for both 2MASS and *WISE* matches. Since we sought to estimate the precision of our catalog, we chose to only use matches within a search radius of $0.5''$. This left us with 69,949 matches between SDSS and *WISE* and 2351 matches between SDSS and 2MASS, 2283 of which were common in both *WISE* and 2MASS. The low number of matches between SDSS and 2MASS is due to the difference in wavelengths and relative depths between the two surveys. The magnitude and flux limits of each survey are shown in Table 1. Because we were assessing the intrinsic precision of the catalog, we chose to apply further cuts to retain only the most pristine detections of QSOs for our analysis. The following criteria were required:

1. SDSS CLEAN = 1,
2. 2MASS CC_FLG = 000,
3. *WISE* CC_FLAG = 0000,
4. *WISE* W1SNR ≥ 30 ,
5. 2MASS J_SNR, H_SNR, or K_SNR ≥ 10 ,
6. 2MASS GAL_CONTAM = 0,
7. *WISE* EXT_FLAG = 0,
8. $\sigma_\alpha < 175 \text{ mas}$ & $\sigma_\delta < 175 \text{ mas}$, and

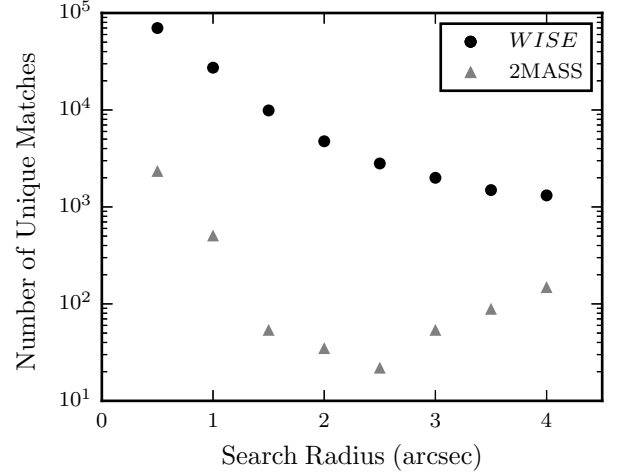


Figure 2. Unique SDSS QSO matches per search radius in 2MASS and *WISE*. Both reach a maximum at a search radius of $0.5''$. The increasing number counts at $> 2''$ for 2MASS indicate resolved neighboring objects being pulled into our search radius for faint QSOs that 2MASS is not able to detect.

9. The closest neighboring primary SDSS object was greater than $6.1''$ (the W1 FWHM) from our source.

These cuts left us with 447 matches for sources with *WISE*+SDSS+2MASS, 4091 matches for sources with only *WISE*+SDSS, and 413 matches for sources with only SDSS+2MASS.

We applied the above algorithm to compute the angular distance measured from the surveys. Distributions of our computed angular distances are shown in Figure 3. The estimated errors in our sample of QSOs are in agreement with, or slightly better than, reported positional uncertainties among each of the three surveys. The largest uncertainties are in our SDSS+2MASS baseline, however, these objects make up a small fraction of our entire proper motion catalog (see Section 3). Figure 3 represents the intrinsic positional errors in each of our fits ($\sim 90 \text{ mas}$ for *WISE*+SDSS+2MASS, $\sim 80 \text{ mas}$ for *WISE*+SDSS, and $\sim 125 \text{ mas}$ for SDSS+2MASS). We add this error, weighted by the time baseline, to the proper motion error for each component.

A number of studies have attempted to correct systematic errors in proper motion catalogs using QSOs (e.g., Röser et al. 2010; Wu et al. 2011; López-Corredoira 2014; Grabowski et al. 2015). We did not observe any large systematics within the *WISE*+SDSS sources, and the small sample size among all other surveys did not allow us to investigate or correct for any potential systematics offsets.

3. DATA

3.1. Building the Catalog

SDSS DR10 boasts over 900 million unique optical sources (after accounting for multiple epochs of photometry)⁸. This study focused on the low-mass stars (point sources) within DR10. We used the following photometric selection criteria, many of which were adapted from

⁸ <https://www.sdss3.org/dr10/scope.php>

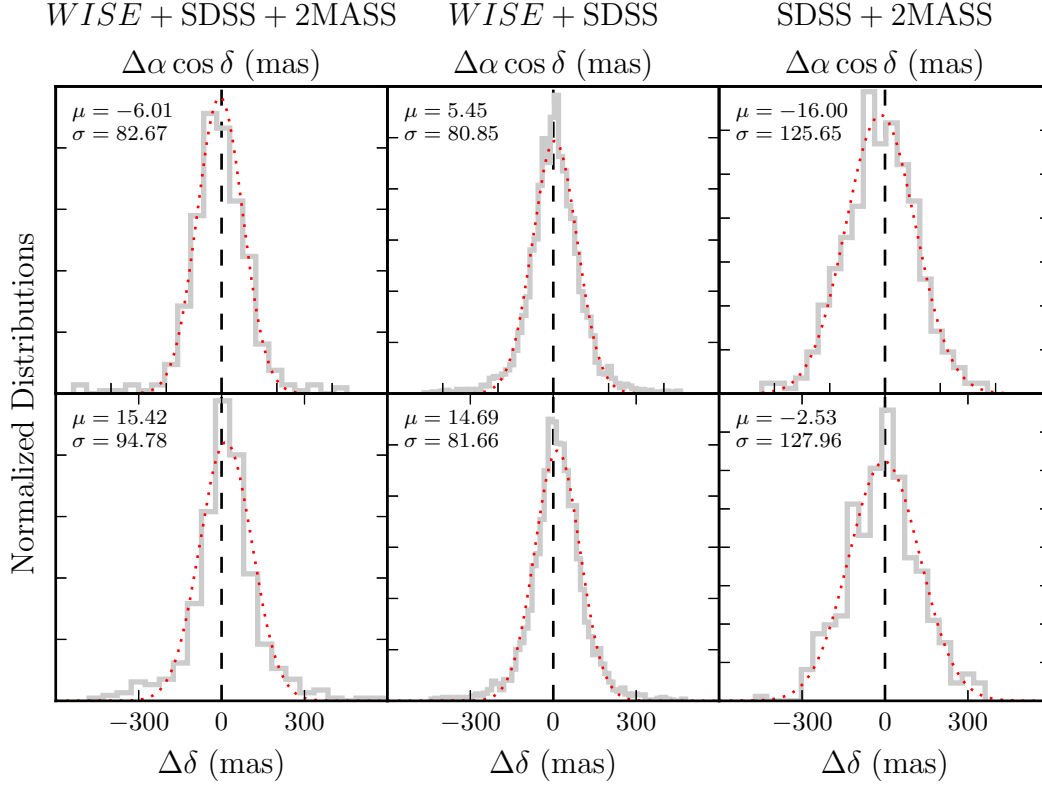


Figure 3. Normalized distributions for the positional difference components among each of the surveys (gray). The best-fit normal distribution is also plotted (red dotted line). The precision tends to be better for observations with a *WISE* epoch. These uncertainties are weighted by the time baseline between observations and added in quadrature to the fitting errors (Section 2.1).

Bochanski et al. (2010, hereafter B10), for our initial search:

1. The photometric objects were flagged as PRIMARY. This was done by querying the STAR sub-catalog of the PHOTOPRIMARY catalog. This also ensured a morphological classification of a point source.
2. The photometric objects fell within the following color limits:

$$\begin{aligned}
 16 < r < 22, \\
 i < 22, \\
 z < 21.2, \\
 r - i \geq 0.3, \text{ and} \\
 i - z \geq 0.2.
 \end{aligned}$$

These color criteria allow for sources slightly bluer than typical dM colors, but were chosen to be inclusive for this stage of the selection process. The *i*- and *z*-band magnitude limits extend past the SDSS 95% completeness ($i < 21.3$ and $z < 20.5$) limits, but we apply additional cuts below. The *r*-band limit removes saturated sources and is slightly brighter than the 95% completeness limit ($r < 22.2$). Although we obtain sources past the 95% completeness limit, we apply more stringent criteria later.

3. We removed sources that had a flag in the *r*-, *i*-, or *z*-bands indicating:

- (a) saturated photometry (SATURATED);
- (b) a significant amount ($>20\%$) of the flux was interpolated from the point spread function (PSF; PSF_FLUX_INTERPRETED)
- (c) centroiding failure caused center to be determined by peak pixel (PEAKCENTER);
- (d) too few good pixels for an interpolated source, causing errors to be underestimated (BAD_COUNTS_ERROR);
- (e) center pixel was too close to interpolated pixel (INTERP_CENTER), and included pixels that were not checked for peaks, potentially saturated (NOTCHECKED);
- (f) after deblending the object did not have a peak (DEBLEND_NOPEAK); and
- (g) contained a pixel interpreted to be part of a cosmic ray (COSMIC_RAY).

4. Sources that indicated centroid was not determined from the *r*-band, but were transformed from some other band (CANONICAL_CENTER), were removed. This was done to ensure objects with reliable *r*-band astrometry, which was used as the calibrator for our SDSS baseline.

These cuts ensured that the *riz* photometry for each source were reliable. Applying these criteria returned 69,792,454 objects.

Using a $6''$ search radius (a similar matching radius to other searches for ultra-cool dwarfs, e.g., Zhang et al.

2009), we matched the SDSS photometric stars to *WISE* and 2MASS sources requiring:

1. $2\text{MASS } J_PSFCHI, H_PSFCHI, \text{ or } K_PSFCHI \leq 2$. This ensures a point-like source morphology, and increases our confidence for a good astrometric measurement.
2. $WISE \text{ } w1RCHI2 \leq 3$. This is the same requirement used to determine a single-point source from a blended object (after deblending) by the *WISE* photometric pipeline.
3. $WISE \text{ } SNR_{W1} > 0$. This removes sources that were not detected in *W1*, but detected in a longer wavelength band. The spectral energy distributions (SEDs) of low-mass stars peak in the near-infrared, therefore, as *W1* was the deepest of the *WISE* bands, low-mass stars should have a detection in *W1* if they have a detection at a longer wavelength.

After this cut we were left with 20,164,221 matches with entries in all three catalogs, 22,741,703 with only *WISE*+SDSS detections, and 2,947,606 with only SDSS+2MASS detections.

3.2. Tracing the Stellar Locus

We were interested in selecting point sources that have the expected colors of main-sequence stars for our initial sample. To ensure this, we computed the expected main-sequence colors for low-mass and very-low-mass stars in the *WISE*, SDSS, and 2MASS photometric systems. We required the following criteria, adapted from Davenport et al. (2014) for low-mass stars, and the AllWISE Explanatory Supplement⁹, to select high quality matches:

1. $13.8 < r < 21.5$ & $\sigma_{r,i,z} < 0.05$, this cut ensured precision photometry within the SDSS 95% completeness limit and saturation limit, and ensured good morphological classification, which has been shown to have an error rate of 5% at $r = 21$ (Lupton et al. 2001).
2. $J > 12$ & $\sigma_J < 0.05$, this cut ensured precision photometry, and should have removed giant stars by using a lower limit on the magnitude (Covey et al. 2008).
3. $W1 < 17.1$ & $\sigma_{W1} < 0.05$, this cut also ensured precision photometry and selected only sources within the AllWISE 95% completeness limit.
4. $|b| > 20^\circ$, this cut reduced extinction effects by removing candidates near the Galactic plane.

After applying the aforementioned cuts, we were left with 9,298,344 sources with only SDSS photometry, 9,890,521 sources with *WISE*+SDSS photometry, and 2,390,962 sources with SDSS+2MASS photometry.

Previous studies have suggested that the majority of point-like sources that meet our color selection criteria

(Section 3.1) are stars versus distant Galaxies (Bochan-ski et al. 2010), however, we wish to be more selective, choosing only high probability stellar candidates for our catalog. To do this, we took our above candidates, selected for their reliable photometry, and examined the stellar locus in bands from all three surveys. Many previous studies have investigated the stellar color locus in numerous colors and a number of photometric systems (see Davenport et al. 2014, and references therein). Instead of using previous results, we chose to measure the color locus from our stellar sample chosen above. We also chose to only measure the locus for the reddest SDSS bands (*riz*) and the deepest 2MASS and *WISE* bands (*J* and *W1*, respectively). Our chosen colors for computing the stellar locus were $r - i$ versus $i - z$, $r - z$ versus $z - J$, and $r - z$ versus $z - W1$.

In small steps of $\delta(\text{color})$, we computed the median absolute deviation from the median and removed objects greater than 5 times the median of the deviations until our distribution converged (i.e. there were no further sources to remove). We then computed the mean and standard deviation of the remaining color distribution. We used a bin size of 0.01 mags for the high density areas (the middle of the distribution), taking steps of 0.01 mags and recomputing. For the red end of the distributions (the low density areas), we increased the bin size to 0.2 mags. Averages and 1σ colors, color steps, bin sizes, and the number of stars in each bin can be found in Appendix A. The visual representation of our computed means and 3σ deviations are shown in Figure 4, where it can be seen that we trace the source density, removing large color outliers.

Due to our initial selection criterion for sources along low-extinction sight-lines ($|b| > 20^\circ$), it is possible that our sample could be biased towards stars with low extinction values. Rather than apply an extinction correction to our stars, we investigated how extinction may bias our selection criteria. To test how accurate our color criteria are for selecting low-mass stars and the effects of interstellar reddening, we applied our cuts to the SDSS DR7 spectroscopic sample of 70,841 M dwarfs (West et al. 2011, hereafter W11), all of which have estimated extinction values from Jones et al. (2011). We investigated the fraction of returned W11 stars, after passing them through our color selection criteria. We applied the cuts above and the cuts from Section 3.1 to the W11 catalog, excluding the requirement that stars have $|b| > 20^\circ$ since we were interested to see how extinction affected our selection method. The total return fraction for stars with $A_V \leq 0.5$ and $A_V > 0.5$ are shown in Table 2 for each combination of color selection criteria. For stars with $A_V \leq 0.5$, our color selection criteria returned $\geq 95\%$ of the W11 inputs stars for all color selection criteria. Even for stars with $A_V > 0.5$ our color selection criteria returned more than 92% of the W11 input stars.

The W11 catalog also contains both disk dwarfs and subdwarfs (Savcheva et al. 2014), populations that can be separated by their metallicity using the ζ -spectroscopic index (e.g., Dhital et al. 2012). To test if our catalog preferentially selects disk dwarfs ($\zeta \geq 0.825$) or subdwarfs ($\zeta < 0.825$), we again investigated the fraction of returned W11 stars after passing them through our color selection criteria, and results are shown in Table 2.

⁹ http://wise2.ipac.caltech.edu/docs/release/allwise/expsup/sec2_4a.html

Table 2
Color Selection Criteria Returns for W11

Color Criteria	Total	Disk Dwarfs	Subdwarfs
$A_V \leq 0.5$			
1 ^a	98.8%	98.8%	99.2%
2 ^b	99.2%	99.2%	98.7%
3 ^c	99.6%	99.6%	95.8%
1+2	98.3%	98.3%	98.3%
2+3	99.0%	99.0%	95.0%
1+3	98.5%	98.6%	95.8%
1+2+3	98.1%	98.1%	95.0%
$A_V > 0.5$			
1 ^a	98.4%	98.4%	98.1%
2 ^b	97.2%	97.2%	96.3%
3 ^c	97.0%	97.2%	94.4%
1+2	96.2%	96.2%	96.3%
2+3	95.9%	96.2%	92.6%
1+3	96.1%	96.2%	94.4%
1+2+3	94.9%	95.2%	92.6%

^a $r - i$ vs. $i - z$ criteria.

^b $r - z$ vs. $z - J$ criteria.

^c $r - z$ vs. $z - W1$ criteria.

Our selection criteria are well-suited for retrieving both disk dwarf and subdwarf populations, with selection of stars in high extinction environments being slightly less reliable, but all above 92%. Our ability to select the vast majority of spectroscopic low-mass stars based on colors alone demonstrate that these color criteria are suitable for selecting photometric low-mass stars, even in regions of moderate extinction.

3.3. Initial Stellar Sample

Applying the color cuts from Figure 4 to our initial stellar sample, we were left with 24,571,934 stars. The color and magnitude range over which each of our matched samples is found is shown in Figure 5. *WISE*+SDSS sources are typically fainter and redder, biasing these matches to later-type stars. SDSS+2MASS matches are bluer, biasing these matches to the earliest type stars in our sample.

Using the above sources as our input catalog, we computed proper motions following Section 2.1. The surveys that went into each proper motion measurement (e.g., *WISE*+SDSS+2MASS or *WISE*+SDSS) are indicated in our catalog by a three bit flag (DBIT), where each bit represents if a survey was used in the proper motion measurement. Descriptions of DBIT and the number of initial sources with each fit are shown in Table 3.

3.4. Reducing Contamination

There are two main issues that can contribute to spurious motion estimates for our stars: 1) nearby sources that can offset the center of the measured PSF if deblending methods fail; and 2) short time baselines that can contain motion caused by parallaxic effects in addition to tangential motion. We will closely examine both of these issues in the following subsections.

3.4.1. Nearby Neighbors

Close neighboring sources are expected to be a contaminant, especially for *WISE* stars due to the large beam size ($\text{FWHM}_{W1}=6.1''$). *WISE* active deblending allows, at most, two components to the PSF fit. The

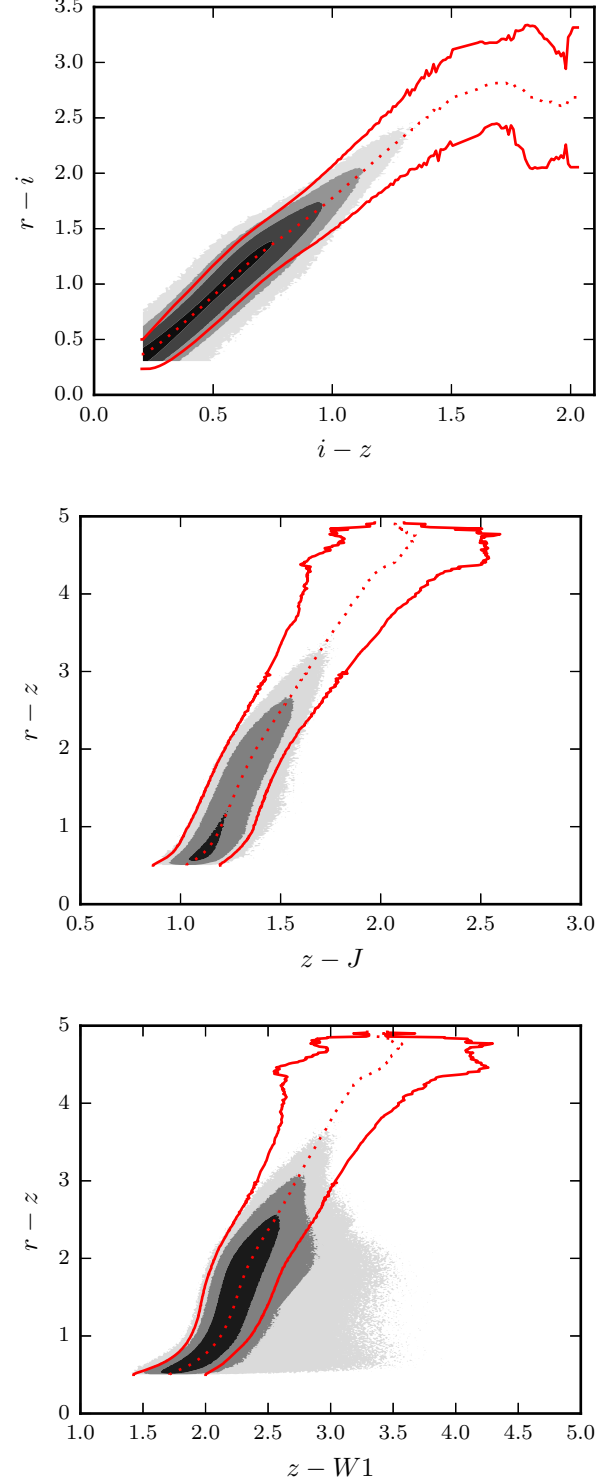


Figure 4. Density plots in *WISE*, SDSS, and 2MASS colors, each bin is $(0.01 \text{ mag})^2$. The first filled contour is drawn at 10 sources per bin, and each subsequent filled contour increases by a factor of 10. Mean colors and 3σ errors used to select our initial stellar sample are also shown (dotted line and solid lines, respectively). Our method well approximates the stellar locus. The points used to draw the limits (dashed and dotted lines) are shown in Appendix A.

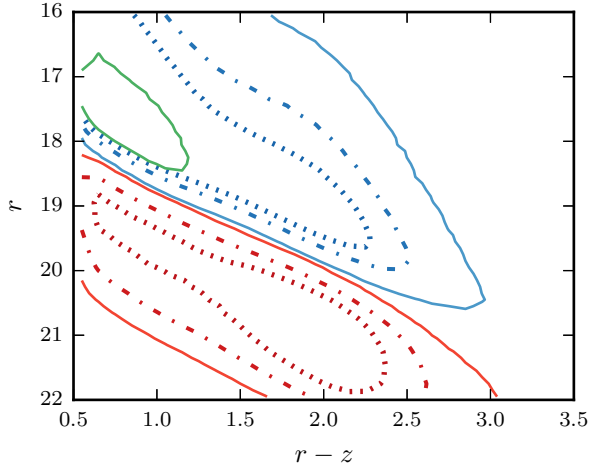


Figure 5. Hess diagram (r vs. $r - z$) with density contours, each bin is $(0.1 \text{ mag})^2$. *WISE*+SDSS+2MASS are drawn in blue, *WISE*+SDSS are drawn in red, and SDSS+2MASS are drawn in green. Contours are drawn at 1000, 5000, and 10000 stars per bin (solid, dash-dotted, and dashed lines, respectively). Each subsample is biased towards a specific brightness and color range.

Table 3
Proper Motion Detection Flags

DBIT	Description	Number
011	SDSS and <i>WISE</i> surveys were used to calculate the proper motions.	<i>initial</i> : 11,911,109 <i>final</i> : 1,801,369
110	2MASS and SDSS surveys were used to calculate the proper motions.	<i>initial</i> : 1,052,228 <i>final</i> : 69,199
111	All three surveys were available and used in the linear fit to calculate proper motions.	<i>initial</i> : 11,608,597 <i>final</i> : 1,733,104
000	SDSS+USNO-B proper motions are available.	<i>final</i> : 6,620,838 <i>unique</i> : 5,216,855

Note. — We show both the initial number of sources that met our first selection criteria (see Section 3), and the final number of stars that went into our catalog.

robustness of this deblending is likely dependent on the flux difference between the two blended sources. To investigate how neighboring objects affect proper motion measurements, we used SDSS CasJobs to select all neighboring primary objects within $15''$ of our sources' SDSS positions. Next, we selected only sources that had one neighboring object within the $15''$ search radius. We expect sources whose photocenters have been moved significantly in *WISE* will have larger fitting errors for sources detected in all three surveys. Figure 6 shows fitting errors as a function of distance to a neighboring object and r -band magnitude difference between our source and the neighboring object. Fitting errors: (1) are significantly larger for brighter neighboring objects, and objects at a distance $\lesssim 8''$; and (2) decrease for extremely close (and bright) neighboring objects ($\lesssim 2''$) due to a reduction in the offset of the measured photocenter from its true position, making the measured positional deviation small.

Figure 6 illustrates that sources with neighboring, bright objects have problematic motion estimates that can be seen in the fitting errors. The following questions must be answered to determine which proper mo-

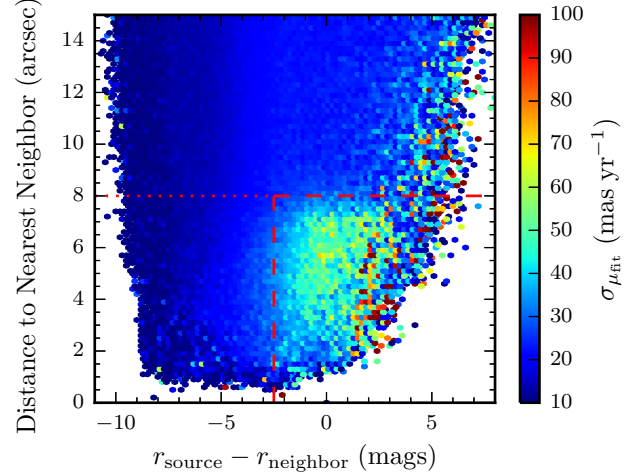


Figure 6. Total proper motion fitting errors for the *WISE*+SDSS+2MASS proper motions as a function of distance to nearest SDSS primary object and magnitude difference between our source and its closest neighbor. Only stars with one neighbor within the search radius are shown, each bin is $0.2 \text{ mags} \times 0.2''$. Stars with fitting errors $> 40 \text{ mas yr}^{-1}$ are suspect due to blending. Dashed and dotted lines correspond to criteria, below which we recomputed proper motions or removed sources (see text for further details). For *WISE*+SDSS+2MASS stars, we recomputed proper motions for stars within the dashed lines. For *WISE*+SDSS sources, we removed stars that had a neighboring object within $\leq 8''$ (dotted line).

tion measurements are reliable: 1) at what distance does a neighboring object affect our measurement; 2) at what magnitude difference does a neighboring object affect our measurement; and 3) what is the fitting error threshold above which a measurement is considered affected (by either neighbors or parallactic effects)? We will explore each of these three questions below.

We expect the error distributions for sources with a neighboring object at a distance $\lesssim 8''$ and $> 8''$ to be different due to the inclusion of more large errors for the distribution with a neighboring object $< 8''$. We require a statistical argument in choosing at what distance a neighboring object affects our measurement. To test for similarity (or difference) in the error distributions, we chose to use the Anderson-Darling test since it is more sensitive to the tails of the distribution, where we expect the larger fitting errors to reside. To determine at which distance a neighboring object affects our proper motion measurement, we selected all sources with $r_{\text{source}} - r_{\text{neighbor}} > -2$. The requirement for sources with $r_{\text{source}} - r_{\text{neighbor}} > -2$ is relatively arbitrary, we are selecting sources where we know fitting errors begin to increase, later we make a more rigorous estimate for $r_{\text{source}} - r_{\text{neighbor}}$. Next, we binned fitting errors in steps of $0.5''$ between $4''$ to $12''$, performing an Anderson-Darling test between adjacent $0.5''$ bins, searching for neighboring distributions with the largest dissimilarity (as traced through a minimum in the p-value). We found a minimum p-value (8×10^{-6}) between the bins from $7.5''$ to $8''$ and $8''$ to $8.5''$, making $8''$ our cutoff value.

Next, to determine at which magnitude difference ($r_{\text{source}} - r_{\text{neighbor}}$) a neighboring object affects our proper motion measurement, we selected all sources with a neighboring object $\leq 8''$. Again, we binned fitting errors

in steps of 0.5 mag between -5 to 3 mags, and performed Anderson-Darling tests between adjacent distributions. We found a minimum p-value (4×10^{-7}) between the bins from $r_{\text{source}} - r_{\text{neighbor}} = -3$ to -2.5 and -2.5 to -2 , making -2.5 our cutoff value. Additionally, we visually inspected a number of stars with proper motion errors between $\sigma_\mu = 30$ – 50 mas yr $^{-1}$ and found that sources with $\sigma_\mu > 40$ mas yr $^{-1}$ tended to be spurious measurements. We chose to recompute proper motions for these stars using just two of the three surveys. Details regarding which surveys were chosen (*WISE*+SDSS or SDSS+2MASS) are described below.

Our method for recomputing proper motions is as follows:

1. We completely removed stars with a neighboring source found within $8''$ and with $r_{\text{source}} - r_{\text{neighbor}} > -2.5$.
2. For stars that do not meet the above criteria, but which have $\sigma_\mu > 40$ mas yr $^{-1}$ in either the α or δ component, we recomputed proper motions by first requiring a minimum signal-to-noise (S/N) in each survey. For *WISE*, we required $S/N_{W1} \geq 3$, and for 2MASS, we required $S/N_{J,H, \text{ or } K_s} \geq 5$. If only one survey met our minimum S/N threshold, we use that survey. If both surveys met our S/N threshold, we used the survey with the highest S/N. To use the *WISE* baseline, we further required a minimum distance to the nearest neighbor be $\geq 8''$.
 - (a) If all the previous criteria of (2) were met, and the highest S/N between both surveys was equal, we used the two surveys with the longest time baseline (either *WISE*+SDSS or SDSS+2MASS).
3. Lastly, we required a time baseline > 1 year between observations. Time baselines shorter than this are susceptible to parallax effects for nearby stars (~ 20 mas yr $^{-1}$ for a star at 100 pc with a baseline of 6 months).

As a final note, the buildup of large errors at a neighboring distance of $\sim 6''$ may also be due to our search radius ($6''$) picking up neighboring objects as the primary if our source becomes too faint at longer wavelengths. Removing these sources ensures both possibilities for contamination are removed from our catalog. Since we are only interested in stars exhibiting *bona-fide* tangential motions, we kept only stars with total proper motions greater than twice their uncertainty ($\mu_{\text{tot}} > 2\sigma_{\mu_{\text{tot}}}$).

4. RELIABILITY OF PROPER MOTIONS

To assess the reliability of our catalog, we compared our proper motions to the LSPM catalog, the SDSS+USNO-B catalog (Munn et al. 2004, 2008, hereafter M04), and the recent deep survey completed within a 1098 deg^2 SDSS footprint (Munn et al. 2014, hereafter M14). The reliability of LSPM should be close to 100% as all these sources have been verified by eye. LSPM stars are selected for larger proper motions (> 150 mas yr $^{-1}$), and the catalog is biased towards brighter stars due to the use of Schmidt plates for the earliest baselines. M04 has time baselines of ~ 50 years, giving it a

high precision, but M04 is not as deep as our catalog, also due to the use of Schmidt plates. M04 has also been matched to a high number of SDSS sources since SDSS was used as the most recent baseline in computing proper motions. Lastly, M14 allows us to test the fidelity of our faintest sources, which LSPM and M04 do not probe. Together, these catalogs allow us to assess the reliability of our sources for the stars with both small and large proper motions, and across all magnitudes.

4.1. Comparison to LSPM

The LSPM catalog contains 61,977 stars in the northern hemisphere with proper motions > 150 mas yr $^{-1}$. The precision of LSPM is ~ 8 mas yr $^{-1}$. LSPM was not specifically designed to target low-mass stars, however, due to its selection of high proper motion stars, it primarily consists of nearby dwarf stars. We matched our catalog to LSPM stars using their 2MASS designations, which produced 12,930 matches. We investigated the agreement between our catalog and LSPM in all three subsamples (e.g., *WISE*+SDSS+2MASS) for each proper motion component, as shown in Figure 7. A small number of large outliers were identified between our *WISE*+SDSS+2MASS and LSPM matches (Figure 7, red circles). We looked through archived images (DSS, SDSS, 2MASS, and *WISE*), since these stars should all have apparent proper motions over the $\gtrsim 20$ year baseline in archived images. The majority of these stars showed proper motions more consistent with our measurements in the archived images. The cause of the spurious measurement in LSPM is unclear, presumably these are bad residual images in the SUPERBLINK pipeline that eluded inspection. Many of these stars also had proper motions consistent with our measurement in another catalog (e.g., USNO-B, M04, NLTT, PPMXL, or URAT1).

We compared the 2σ agreement in both proper motion components to test the absolute agreement between our catalog and LSPM. For our *WISE*+SDSS+2MASS matches, we found 98% agreement between our catalog and LSPM. For our *WISE*+SDSS and SDSS+2MASS matches this agreement was 97% and 96%, respectively. All agreements increase to 99% at 3σ . All our *WISE*+SDSS matches to LSPM were recomputed values (see Section 3.4.1), since these stars are all bright enough to have an entry in 2MASS. This comparison shows our catalog is reliable for the fastest moving stars.

4.2. Comparison to M04

Due to the sensitivity of M04, spurious proper motion estimates are expected for fainter stars. To compare our catalog to M04 we needed to determine which sources were reliable. We matched our catalog to the Munn et al. (2004) catalog (contained within SDSS CasJobs as the PROPERMOTIONS table) by SDSS OBJID. We chose to use only sources with “good” proper motions, adopting the constraints from Kilic et al. (2006):

1. $\text{DIST22} > 7$, the nearest neighboring objects with $g < 22$ is more than $7''$ away.
2. $\text{MATCH} = 1$, there is a one-to-one match with the USNO-B object and the SDSS object.

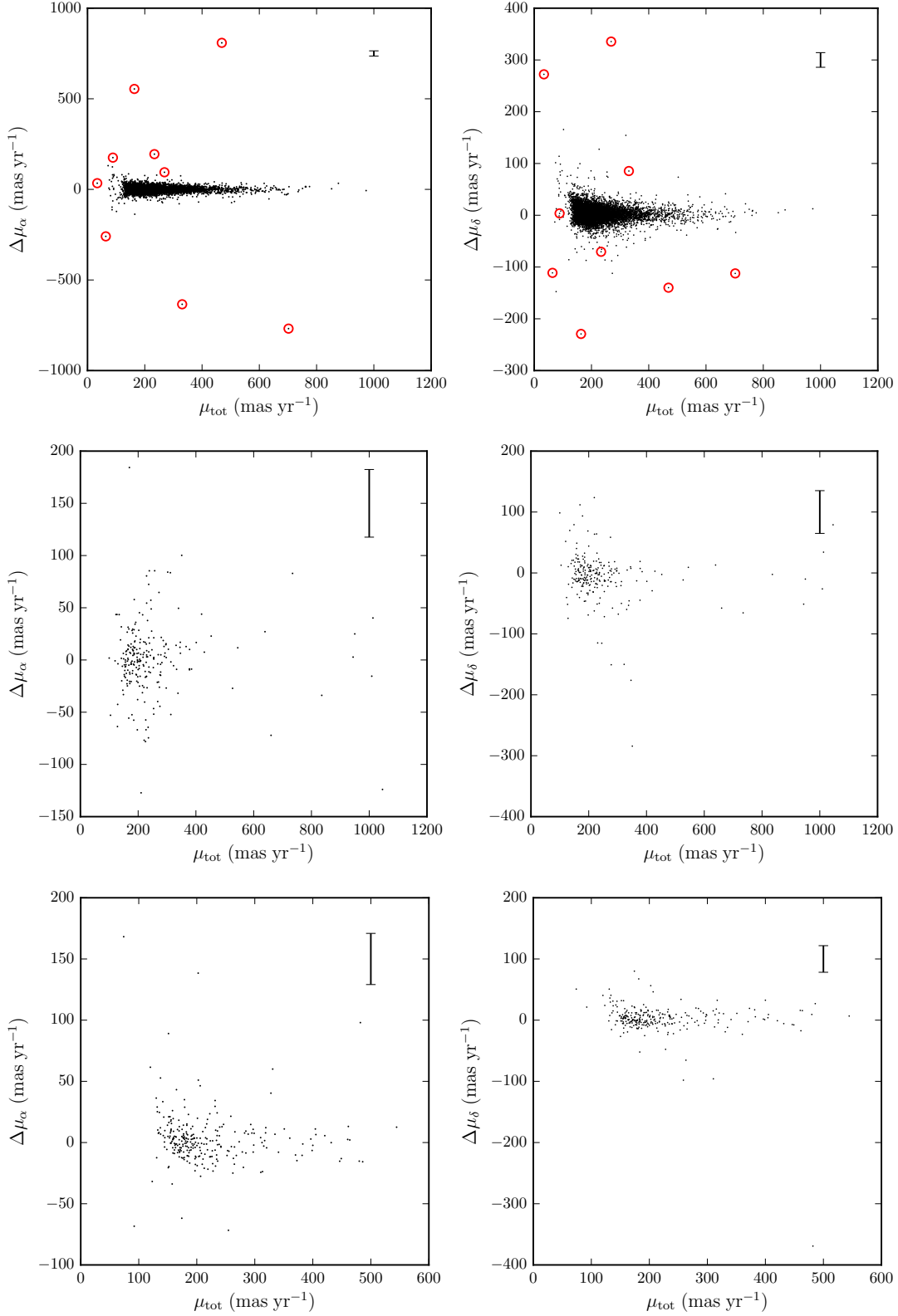


Figure 7. Residual proper motion ($\mu_{\text{this study}} - \mu_{\text{LSPM}}$) for both components (μ_α and μ_δ) as a function of our total proper motion. Typical errors are shown in the top right corners. *Top*: WISE+SDSS+2MASS stars compared against LSPM. Overall, our stars show good agreement with LSPM, however, a small number of outliers were identified and investigated (red circles, see text for details). *Middle*: WISE+SDSS stars compared to LSPM. Again, there is good agreement between our stars and LSPM, with the outliers typically due to bad astrometry in one of our surveys. *Bottom*: SDSS+2MASS stars compared to LSPM. Similar to our WISE+SDSS stars there is good agreement with LSPM, with the outliers once again due to bad astrometry in one of our surveys.

3. $n\text{FIT} = 6$, the object was detected in all five USNO-B plates, as well as detected in SDSS
4. $\text{SIGRA} < 525$, and $\text{SIGDEC} < 525$, the RMS residuals for the proper motion fits were less than 525 mas in both components.

These criteria yielded 919,867 matches between our SDSS sources and M04 sources.

Since M04 is biased towards brighter objects, we chose to compare it to sources that have proper motions measured using all three surveys (*WISE*+SDSS+2MASS). There were 842,776 matched stars with *WISE*+SDSS+2MASS measured proper motions, making up the bulk of the matches between our catalog and M04. We investigated the residuals between our computed proper motions and those from M04 as a function of color and magnitude (Figure 8). There is a strong increase in the magnitude of the residuals for fainter stars and bluer stars. The correlation between apparent magnitude and $r - z$ color is due to bluer stars peaking in the optical (and NIR), while getting fainter at *WISE* bands. The combined filter set of *WISE*+SDSS+2MASS is more sensitive to stars that peak towards the red end of the NIR, out to $\sim 4 \mu\text{m}$. We expect M04 to be more sensitive to bluer stars, however, we can examine the proper motion distributions for these faint sources to determine whether ours, or the M04 values are more consistent with expectations.

In general, we expect fainter stars to be more distant, and therefore exhibit smaller proper motions. Our proper motions for fainter sources tend to be higher than those from M04, as can be seen in Figure 8 (positive residuals). We performed a linear fit to the residuals in color-magnitude space, fitting to where the residuals became higher than 20 mas yr^{-1} (dashed line, Figure 8), and where the residuals became higher than 10 mas yr^{-1} (dash-dotted line, Figure 8). Our results are shown in Figure 8, with the proper motions separated by,

$$r \leq 16.65 + 1.435(r - z) \quad \text{for } \Delta\mu_{\text{tot}} < 20 \text{ mas yr}^{-1}, \quad (11)$$

and

$$r \leq 15.34 + 1.896(r - z) \quad \text{for } \Delta\mu_{\text{tot}} < 10 \text{ mas yr}^{-1}. \quad (12)$$

As stated above, due to the difference in wavelengths between each of the surveys used in calibrating our catalog, we expect fainter, redder sources to be more easily detectable than fainter, bluer sources. This is exhibited in Figure 8, where our proper motion errors also begin to grow large at approximately the same limit that our residuals began to increase. Therefore, both our proper motions and our proper motion errors increase at the same limit, potentially keeping our measurements to within errors but with less precision. To quantify the reliability of our catalog, we compared the 2σ and 3σ agreement for both proper motion components for matched stars, both fainter and brighter than equation (11), and as a function of color, the results of which are shown in Table 4.

In general, there is good agreement between our measurements and the M04 catalog. This agreement is less certain for stars fainter than equation (11), but increases

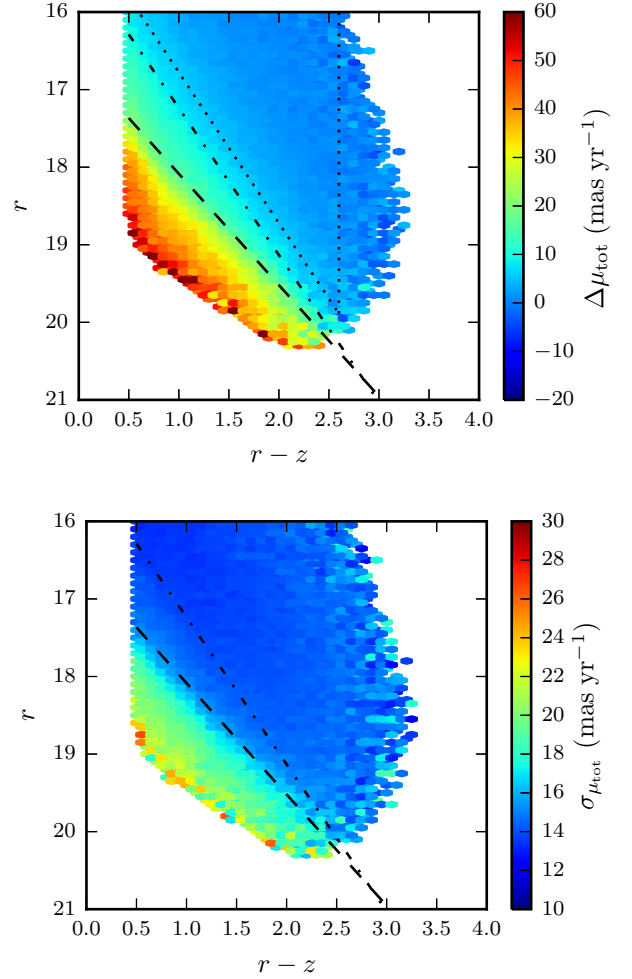


Figure 8. *Top:* Residual total proper motion ($\Delta\mu_{\text{tot}} = \mu_{\text{tot}}(\text{WISE+SDSS+2MASS}) - \mu_{\text{tot}}(\text{M04})$) as a function of source r -band magnitude and $r - z$ color, each bin is $(0.1 \text{ mags})^2$. The performance of our catalog is tightly correlated with source color and magnitude. The dashed line represents the limit above which residuals become $> 20 \text{ mas yr}^{-1}$, and the dash-dotted line represents the limit above which residuals become $> 10 \text{ mas yr}^{-1}$. More stringent criteria used to investigate the reliability of the M04 catalog (Section 5) are also shown (dotted lines). *Bottom:* Total proper motion error ($\sigma_{\mu_{\text{tot}}}$) as a function of source r -band magnitude and $r - z$ color, each bin is $(0.1 \text{ mags})^2$. The dashed and dash-dotted lines are the same as the top. Our measurement uncertainty becomes large at the same limit that residuals begin to grow larger than 20 mas yr^{-1} . The performance of our catalog is tightly correlated with source color and magnitude, due to our inability to probe small proper motions expected for more distant (fainter) sources. Although we lose precision at fainter magnitudes, our proper motion measurements are still consistent to within the errors.

for redder colors fainter than this limit. Since the performance of the USNO-B survey is also expected to deteriorate at fainter magnitudes ($V \gtrsim 19$; Lépine & Shara 2005; Dong et al. 2011), we can expect sources in disagreement to be a mixture of spurious measurements in our catalog and in USNO-B. This is left as a cautionary note, as many of the stars fainter than equation (11) will have real proper motions. We do not remove these stars, as many of them will be true measurements, we instead augment them with a second measurement from M04 (see Section 5).

Table 4
Agreement with other Proper Motion Catalogs

Comparison Catalog	Subsample	$r - z$	2σ Agreement	3σ Agreement
M04	<i>WISE</i> +SDSS+2MASS	All	86%	95%
M04	SDSS+2MASS	All	28%	72%
M04	<i>WISE</i> +SDSS	All	15%	50%
M14	<i>WISE</i> +SDSS+2MASS	All	82%	94%
M14	SDSS+2MASS	All	21%	74%
M14	<i>WISE</i> +SDSS	All	25%	63%
M14	<i>WISE</i> +SDSS	> 3	82%	93%
$r \leq 16.65 + 1.435(r - z)$				
M04	<i>WISE</i> +SDSS+2MASS	All	94%	99%
M04	SDSS+2MASS	All	87%	97%
M04	<i>WISE</i> +SDSS	All	46%	63%
M14	<i>WISE</i> +SDSS+2MASS	All	95%	99%
M14	SDSS+2MASS	All	69%	95%
M14	<i>WISE</i> +SDSS	All	57%	77%
$r > 16.65 + 1.435(r - z)$				
M04	<i>WISE</i> +SDSS+2MASS	All	46%	75%
M04	<i>WISE</i> +SDSS+2MASS	> 1	50%	77%
M04	<i>WISE</i> +SDSS+2MASS	> 1.5	52%	78%
M04	<i>WISE</i> +SDSS+2MASS	> 2	55%	80%
M04	SDSS+2MASS	All	13%	66%
M04	<i>WISE</i> +SDSS	All	13%	49%
M04	<i>WISE</i> +SDSS	> 2	28%	59%
M14	<i>WISE</i> +SDSS+2MASS	All	60%	84%
M14	<i>WISE</i> +SDSS+2MASS	> 3	93%	98%
M14	<i>WISE</i> +SDSS	> 3	80%	92%

A similar comparison can be made between our *WISE*+SDSS and SDSS+2MASS proper motions and M04. However, these samples are limited in that they are typically bluer (SDSS+2MASS) or fainter (*WISE*+SDSS) than our *WISE*+SDSS+2MASS stars. These comparisons are also shown in Table 4. In general, agreement is again better for stars brighter than equation (11), and for redder stars.

We further investigated how our agreement scaled with proper motion errors among all three subsamples, as is shown in Figure 9. Stars with larger proper motion errors (e.g., fainter stars and stars with smaller time baselines) tend to have to be closer to our 3σ limit, or be in disagreement. The majority of stars across all three subsamples tend to be within 3σ agreement, a proper motion error cut may be useful in selecting higher confidence proper motions. It is difficult to say if the disagreement between the faintest sources in our catalog (and M04) is a limitation of M04 or our catalog. To answer this question, we require a proper motion catalog as deep (or deeper) than our catalog.

4.3. Comparison to M14

The M14 proper motion survey covers only a small footprint within SDSS, but provides proper motions down to $r \approx 22$. This catalog has time baselines $\gtrsim 5$ years with a precision of $\sim 10 \text{ mas yr}^{-1}$. We applied all the M14 suggested quality cuts (summarized in Table 1 of M14). Although these cuts were designed to remove spurious proper motion measurements, M14 found that they were only able to remove $\sim 50\%$ of the “bad” detections, while retaining $> 97.6\%$ of the “good” detections (from comparison stars between M14 and LSPM). Therefore, it is possible that some of the proper motions retrieved

are spurious measurements. The fidelity of the proper motions within this catalog have not been independently verified, therefore, the following analysis should be taken as both an investigation into the reliability of our catalog as well as M14.

We matched our catalog to M14 by SDSS OBJID, giving us 510,799 matches. We performed an analysis similar to our comparison to M04 above. We began with a comparison of our *WISE*+SDSS+2MASS stars, which made up 246,678 of our matches. Figure 10 shows the total proper motion residuals ($\mu_{\text{tot}}(\textit{WISE}+\text{SDSS}+2\text{MASS}) - \mu_{\text{tot}}(\text{M14})$) as a function of r -band magnitude and $r - z$ color. Equations (11) and (12) from our M04 analysis represent similar reliability for M14, past the magnitude limit that M04 was able to probe. Reliability tends to increase for stars with $r - z > 3$.

We again explored the 2σ and 3σ agreement between both proper motion components for M14 and our catalog (see Table 4). Agreements between our *WISE*+SDSS+2MASS measurements and M14 are similar to those found with M04, except for the *WISE*+SDSS stars which are in better agreement than those found against M04 with a larger number of stars (261,141). Agreement is also better for redder stars (stars with $r - z > 3$), the majority of which were fainter than equation (11) from Section 4.2. This shows that our *WISE*+SDSS sources are typically too faint to have reliable proper motions in M04. In general, our proper motions across all three subsamples appear to be reliable (to within our uncertainties) up to our magnitude limit of $r = 22$, with redder sources having higher reliability. Figure 11 shows how proper motion agreement scales with proper motion error (similar to Figure 9). We find slightly better agreement for stars with larger

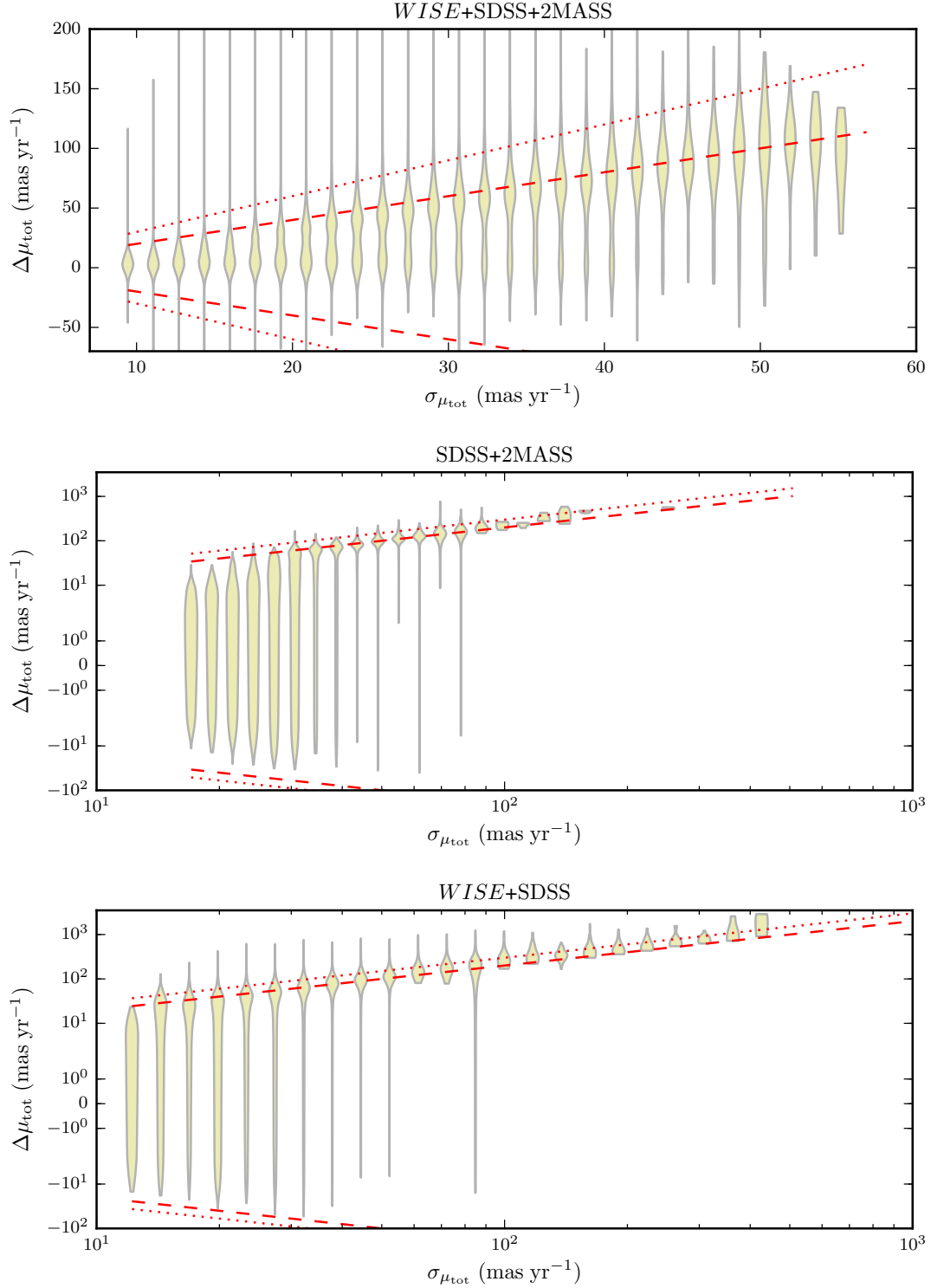


Figure 9. Violin plots for residual total proper motion ($\Delta\mu_{\text{tot}} = \mu_{\text{tot}}(\text{WISE+SDSS+2MASS}) - \mu_{\text{tot}}(\text{M04})$) as a function of total proper motion error. These plots show the relative distribution of stars for each error bin. The dashed and dotted line represent 2σ and 3σ agreement, respectively. *Top:* The majority of WISE+SDSS+2MASS stars are all in 3σ agreement with M04, agreement is better for small errors. *Middle:* The SDSS+2MASS stars tend to be in better agreement for smaller errors. From our error distribution (Section 6), the majority of our sources should have reliable (within 3σ) proper motions. *Bottom:* The WISE+SDSS stars also tend to be in better agreement for smaller errors. From our error distribution (Section 6), many sources tend to straddle the limit of 3σ reliability. These stars also represent the faintest sources, and thus suffer from small number statistics when matched to M04.

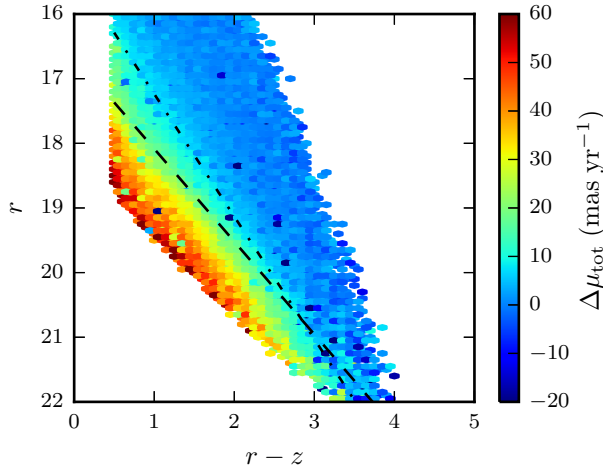


Figure 10. Same as Figure 8, but residuals with M14. Equations (11) and (12) approximately trace the same levels of reliability for M04 and M14, with reliability increasing for fainter, redder stars ($r - z > 3$).

proper motion errors than we did for M04. As stated above, cutting on proper motion errors can yield higher reliability.

Our comparison with LSPM shows us that our catalog is reliable for the brightest and faster moving stars. The majority of stars with discrepant proper motions were found to have more reliable measurements in our catalog. Comparisons with M04 and M14 show that our catalog tends to be more reliable for brighter sources, but reliability remains high for fainter, redder stars. Rather than make further cuts on our catalog, we summarize our findings and use the results of our comparisons to suggest selection criteria to obtain a clean sample in Section 6.

5. AUGMENTING OUR PROPER MOTIONS WITH SDSS+USNO-B

Our combined *WISE*+SDSS+2MASS proper motions are mostly sensitive to faster moving ($\mu_{\text{tot}} > 20 \text{ mas yr}^{-1}$) and redder stars. To make the most complete set of proper motions and to ensure the highest completeness for low-mass stars within the SDSS photometric sample, we require a baseline more sensitive to slower moving (tangentially) stars, or disk stars. The ideal remedy is M04, which has a higher precision ($\sigma_{\mu_{\text{tot}}} \lesssim 4 \text{ mas yr}^{-1}$), but is more sensitive to brighter sources (see Section 4). To augment our derived proper motions with those from M04, we must first choose criteria that select the most reliable proper motions from M04. A number of different criteria have been proposed for selecting a “clean” sample of SDSS+USNO-B stars (e.g., Kilic et al. 2006; Dhital et al. 2010; Dong et al. 2011; West et al. 2011). We performed an in-depth exploration into the effect of different criteria on selecting a clean sample.

The most important parameters within the M04 catalog for our investigation were (taken from SDSS SkyServer¹⁰ PROPERMOTIONS CasJobs table):

1. MATCH, the number of objects in USNO-B that matched this object within a $1''$ radius. If negative,

then the nearest matching USNO-B object itself matched more than 1 SDSS object.

2. SIGRA and SIGDEC, the RMS residuals for the proper motion fit (in R.A. and Dec., respectively).
3. NFit, the number of detections used in the fit including the SDSS detection (thus, the number of plates the object was detected on in USNO-B plus one).
4. O and J, the recalibrated USNO-B *O* and *J* magnitudes, respectively, recalibrated to SDSS *g*.

We chose to keep the criterion $\text{DIST22} > 7$ since this criterion is common among all methods for selecting a “clean” sample. We explored each of the criterion outlined in the aforementioned studies, seeing how proper motion agreement changed with each criteria.

To select a clean sample, we chose a subset of our color-magnitude space where the absolute residuals with M04 were typically $< 10 \text{ mas yr}^{-1}$. The region we selected from is shown in Figure 8. In this region, we had 98% agreement between M04 and our *WISE*+SDSS+2MASS proper motions at 2σ (with 381,188 stars). Next, we performed a match between our catalog to M04 with no requirement on any of the above parameters. This match gave us 495,385 stars within the aforementioned color-magnitude space. We performed a number of tests, using criteria recommended in the various papers listed above, and compared the 2σ agreement between ours and the M04 proper motion components. The results of our comparisons are summarized in Figure 12, and our recommended criteria for selecting high reliability candidates is:

1. $\text{DIST22} > 7$ and,
2. $\text{SIGRA} < 525$ and $\text{SIGDEC} < 525$ and,
3. ($\text{NFit} = 6$ and $\text{MATCH} \geq 1$) or
4. ($\text{NFit} = 5$ and $\text{MATCH} = 1$ and [$O < 2$ or $J < 2$]).

Using these criteria should yield proper motions with more than 95% confidence. Another optional cut is to remove (redder) objects with $r - z > 3$, which typically have less reliable proper motions, however, these objects make up only a small fraction of the objects within M04 ($< 0.2\%$).

We chose to supplement our proper motions with those from M04, applying all of the above criteria outlined, and also requiring a minimum total proper motion greater than two times the combined total proper motion error ($\mu_{\text{tot}} > 2\sigma_{\mu_{\text{tot}}}$). This gave us 6,620,838 stars, 5,216,855 of which we did not have a prior measurement for. The final number of stars in our catalog for each subsample is listed in Table 3.

6. THE MoVeRS CATALOG

Our goal was not to construct a “complete” proper motion catalog, rather, we have attempted to build a catalog of low-mass stars with high-fidelity proper motion measurements. We expect our catalog to be more “complete” at the red end of the main-sequence than most previous proper motion catalogs due to the use of deeper

¹⁰ <http://skyserver.sdss.org/dr12/en/help/browser/browser.aspx?&history=description+ProperMotions+U>

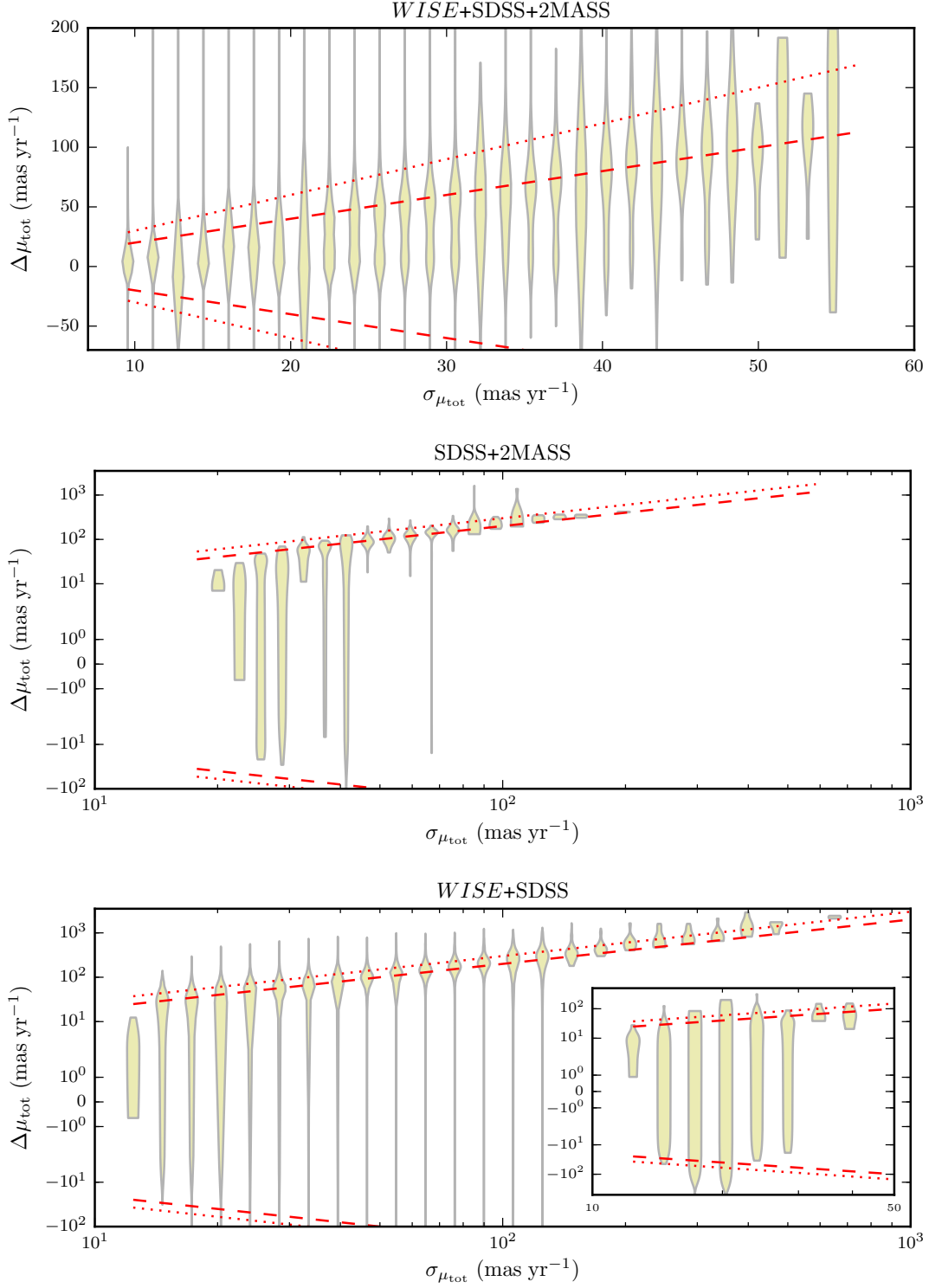


Figure 11. Same as Figure 9, but for M14 matches. *Top:* The *WISE*+*SDSS*+2*MASS* stars tend to have more scatter in their residuals than the M04 stars, however, the majority are in 3σ agreement with M14. *Middle:* The *SDSS*+2*MASS* stars tend to be in better agreement for smaller errors, similar to M04 matches. *Bottom:* The *WISE*+*SDSS* stars also tend to be in better agreement for smaller errors, similar to M04 matches. The inset plot shows only stars with $r - z > 3$, which are typically more reliable.

	NFit= 4	NFit= 5	NFit= 6	525 < (SIGRA & SIGDEC) < 1000	$O < 2$ or $J < 2$	MATCH > 1
NFit= 4	94.9% (19279)					
NFit= 5		96.1% (88247)				
NFit= 6			98.1% (381188)			
525 < (SIGRA & SIGDEC) < 1000	35.5% (34)	39.3% (89)	75.5% (204)	75.5% (204)		
$O < 2$ or $J < 2$	93.1% (13340)	96.0% (66019)	96.1% (538)	50.0% (2)	97.3% (518)	
MATCH > 1	88.3% (571)	88.7% (477)	97.9% (662)	100.0% (2)	100.0% (5)	98.6% (639)

Figure 12. Table showing the percentage of stars that had a 2σ agreement in both proper motion components (α and δ) between our *WISE*+SDSS+2MASS proper motions and those from M04, as a function of M04 parameters. The number of stars that met each criteria are listed below the percentage in parenthesis. Colors represent our limits for selecting: 1) “good” criteria (green); 2) “bad” criteria (red); 3) baseline, or starting, criteria (blue); and 4) criteria that did not include enough stars to be meaningful (light gray). Default criteria, unless changed, were: 1) NFit = 6; 2) SIGRA & SIGDEC < 525; and 3) MATCH = 1.

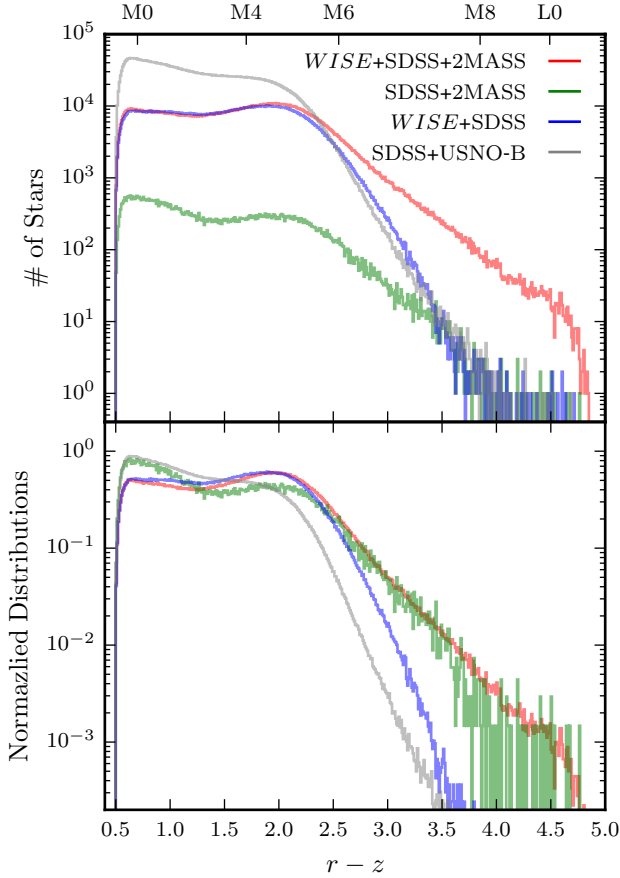


Figure 13. $r - z$ distributions for each subsample in our catalog. Approximate spectral types taken from Hawley et al. (2002) and Bochanski et al. (2007). M04 and our SDSS+2MASS distributions typically include more bluer stars, while proper motions measured with *WISE* typically include more redder stars.

surveys, specifically in the IR. To illustrate this point, we show the $r - z$ color distribution for each of our subsamples (e.g., *WISE*+SDSS+2MASS or SDSS+USNO-B) in Figure 13. Our *WISE*+SDSS+2MASS baseline contains a large number of star with $r - z > 2.5$, and our *WISE*+SDSS subsample also contains more stars with $r - z > 2.5$ than our M04 stars, which peak at a spectral type of \sim M4. Our newly computed proper motions will identify many new very-low-mass stars with $r - z > 2.5$ (spectral types later than \sim M6). The schema for our catalog can be found in Appendix C. Proper motions and errors for each of the subsamples in our catalog are shown in Figure 14. The extremely wide wings for our *WISE*+SDSS and SDSS+2MASS matches are due primarily to stars with short time baselines (< 3 years), which typically overestimate proper motions.

A small number of our stars have high proper motions ($\mu_{\text{tot}} > 1000 \text{ mas yr}^{-1}$; $\sim 0.5\%$). Some of these stars are due to our large search radius ($6''$), which may pull in neighboring objects. Our color selection criteria should remove a number of these, however, in crowded fields (e.g., within the Galactic plane), these objects are more prominent. Rather than remove fast moving objects, since many of them will be true detections, we recommend a conservative cut to remove potential outliers is to eliminate stars near the Galactic plane (e.g.,

$|b| < 20^\circ$).

Another potential cut is to remove objects that have appeared to move a distance close to our search radius over the time baseline (e.g., objects that have moved $\sim 6''$ within a 1 year period). We plan to determine the validity of these high proper motions sources in a future study. Also, selecting stars that either satisfy equation (11) or (12) can yield higher reliability proper motions, but is biased towards selecting stars with all three epochs. Lastly, selecting stars with smaller proper motion errors ($\sigma_{\mu_{\text{tot}}} \lesssim 60 \text{ mas yr}^{-1}$), specifically for the *WISE*+SDSS and SDSS+2MASS subsamples can increase reliability. The M04

7. DISCUSSION

This paper presents an improved proper motion catalog for low-mass stars, specifically, completing the red end of the low-mass sequence. Based off our color selection, this catalog spans from late K dwarfs to early L dwarfs. In particular, this catalog will allow unprecedented studies of subdwarfs and potential halo stars. To show the relative populations of stars within our catalog, we include reduced proper motions (RPMs; Luyten 1922), given as

$$H_r = r + 5 + 5 \log \mu = M_r - 3.25 + 5 \log v_T, \quad (13)$$

where μ is the total proper motion in arcsec yr^{-1} , and v_T is the heliocentric tangential velocity in km s^{-1} given by $v_T = 4.74 \times (\mu \cdot d)$, where d is the distance in parsecs. RPM diagrams for each of our four subsamples are shown in Figure 15. To segregate different kinematic groups, we have drawn a line at $v_T = 180 \text{ km s}^{-1}$, the approximate limit which differentiates disk stars from subdwarfs (Sesar et al. 2008). Although subdwarfs may scatter above the 180 km s^{-1} line, disk dwarfs are not typically found below the 180 km s^{-1} line (Dhital et al. 2010).

The SDSS+USNO-B stars are primarily earlier type disk stars. Our *WISE*+SDSS+2MASS stars are also primarily disk dwarfs, but peak at redder colors, and are more complete (and reliable) at the reddest end of the main-sequence. Our SDSS+2MASS and *WISE*+SDSS baselines appear to probe bluer and redder subdwarf populations, respectively.

We have identified a number of science questions which can be investigated with this catalog:

1. Identify SDSS spectroscopic high-proper motion low-mass stars to find hypervelocity candidates (Favia et al., submitted.).
2. Identify extremely low-mass, common proper motion binaries.
3. Investigate Galactic kinematics for the lowest-mass main-sequence members.
4. Identify low-mass field stars with infrared excesses.
5. Confirm pervious catalogs of wide-binaries (e.g., Dhital et al. 2015).

With current and future efforts multi-epoch surveys, such as *Gaia* and LSST, this catalog will also prove invaluable as a calibrator for the reddest stellar populations within these surveys.

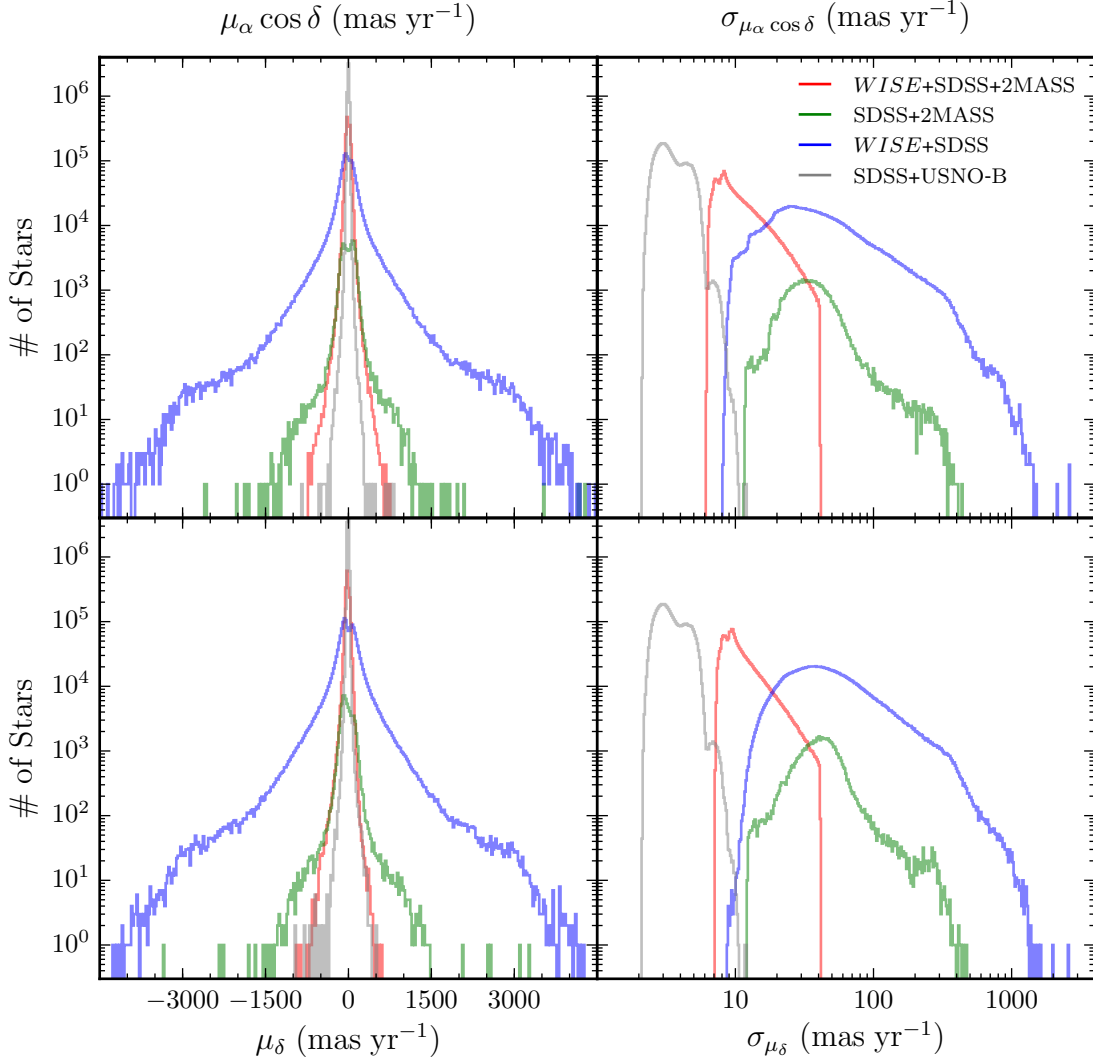


Figure 14. Proper motion and proper motion error distributions for our catalog. The vast majority of our catalog is comprised of stars with $\mu_{\text{tot}} < 1000 \text{ mas yr}^{-1}$ (99.5% of the entire catalog).

7.1. Common Proper Motion Binaries: Investigating the SLoWPoKES-II Catalog

To demonstrate the utility of MoVeRS, we matched our catalog to the second release of the Sloan Low-mass Wide Pairs of Kinematically Equivalent Stars (SLoWPoKES-II; Dhital et al. 2015), a sample of wide binaries identified without proper motions. This catalog is an extension of the study from Dhital et al. (SLoWPoKES-I; 2010), where it was shown that wide-binaries with separations less than $\sim 20''$ could be identified based off similar distances, but without the need for proper motions. There were 260 matches between the two catalogs. Figure 16 shows the distributions for the proper motion components between the primary and secondary, the distribution of equation (6) from Dhital et al. (2010), a measure of the weighted difference in both proper motion components given as

$$\chi_{\mu} = \left(\frac{\Delta\mu_{\alpha}}{\sigma_{\Delta\mu_{\alpha}}} \right)^2 + \left(\frac{\Delta\mu_{\delta}}{\sigma_{\Delta\mu_{\delta}}} \right)^2. \quad (14)$$

The fraction of matches that met the criteria of reliable proper motions binaries ($\chi_{\mu} \leq 2$; Dhital et al. 2010) was 38%. If we restrict this analysis to pairs that have proper motions with all three epochs (i.e. WISE+SDSS+2MASS; 127 pairs), this fraction increase to 47%.

The original SLoWPoKES catalog did not have a formal constraint on average distance due to the fact that the range of spectral types (mid-K to mid-M) made the catalog sensitivity a function of color and distance. It was found that reliability was higher for stars with $d \lesssim 1200 \text{ pc}$, due to smaller photometric distance uncertainties. Since SLoWPoKES-II has no constraint on average distance, we chose to explore how pair fidelity corresponded with distance. Figure 17 shows the distribution of both high-fidelity pairs ($\chi_{\mu} \leq 2$) and low-fidelity pairs ($\chi_{\mu} > 2$). High-fidelity pairs are primarily found within 1200 pc, with fidelity becoming noticeably worse at larger distances.

We chose to investigate how angular separation between the primary and secondary component affected the likelihood of pairs having common proper motions. From

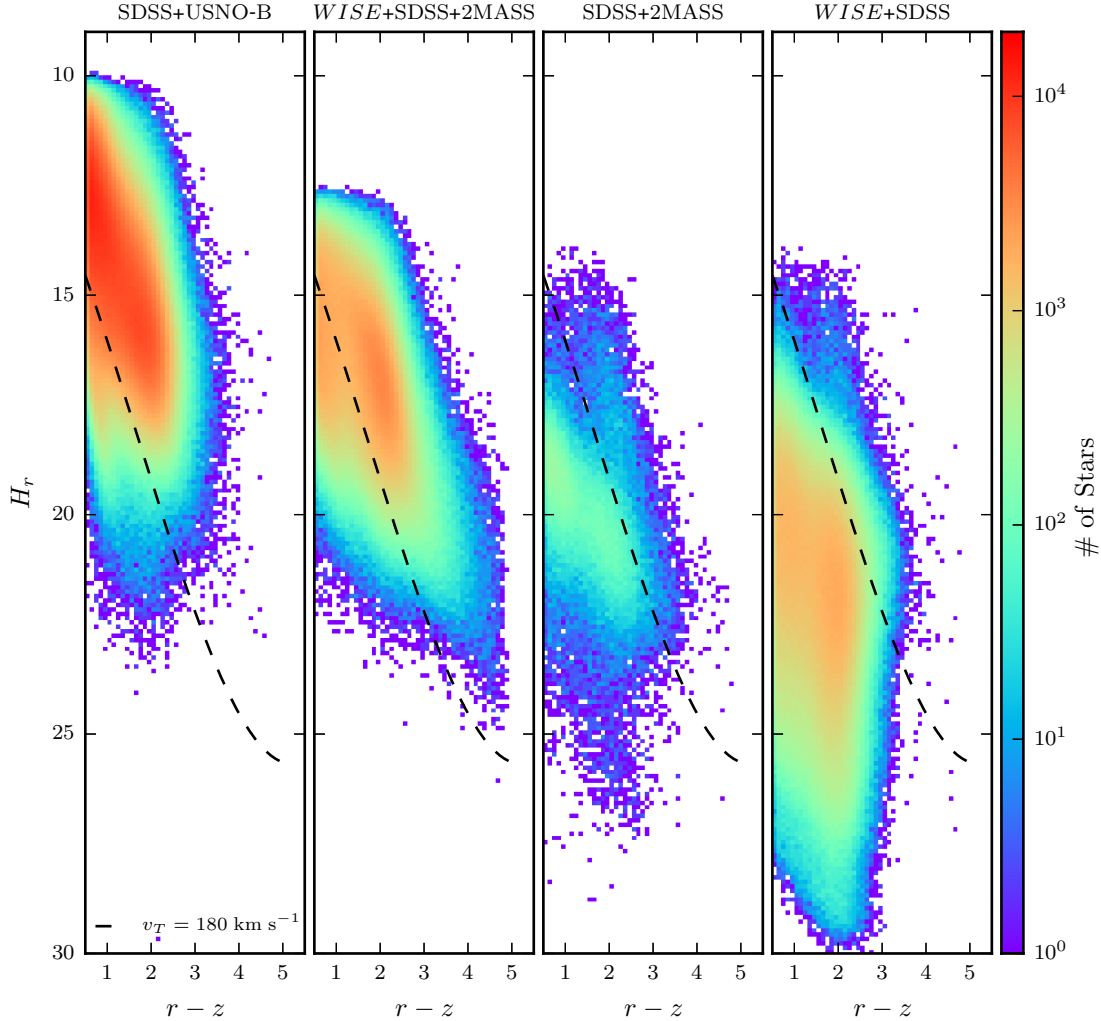


Figure 15. Reduced proper motion diagrams for the four sub-samples included in our catalog, each bin is $(0.1 \text{ mags})^2$. The dashed line represent a tangential velocity of 180 km s^{-1} , which separates disk stars from halo stars (Sesar et al. 2008). Our catalog provides one of the largest samples of high-confidence subdwarfs (stars below the dashed line). The M04 source at $r - z \approx 2$, $H_r \approx 30$ appears to have a spurious proper motion (as observed in archived images).

the results of Dhital et al. (2010) and Dhital et al. (2015), we expect closer pairs to have a higher probability of being true binaries. However, we only have the ability to probe pairs with separations $\gtrsim 8''$, except for a small subset of objects matched in SDSS+2MASS. To investigate reliability as a function of pair separation, we calculated the fraction of reliable pairs in a moving $1''$ bin and computed binomial uncertainties, using only pairs with an average distance $\leq 1200 \text{ pc}$ since reliability was shown to decrease significantly past this point. Our results are shown in Figure 18; as expected, proper motion reliability decreases with angular separation; for sources with angular separations $> 15''$, we find reliability drops to zero. Due to the small sample size of our matched pairs, we do not attempt to make any claims on the overall reliability of SLoWPoKES-II; this exercise was simply used to show the applicability of our catalog. From our initial results, coupled with the fact that the distribution of angular separations in the SLoWPoKES-II catalog peaks at separations $< 8''$, we expect many of the pairs to be *bona-fide* binaries. Choosing pairs with smaller average distances and smaller angular separations can help im-

prove the fidelity of the sample.

8. SUMMARY

We have created a catalog containing 8,735,004 proper motion verified photometric low-mass stars. Proper motions were computed using the *WISE*, SDSS, and 2MASS surveys (3,518,150 stars), and augmented with proper motions from SDSS+USNO-B (5,216,854 stars; Munn et al. 2004, 2008). All stars were required to have a total proper motion greater than twice the uncertainty in their measurement, thus ensuring high-fidelity main-sequence stars. The estimated precision of our catalog is $\sim 10 \text{ mas yr}^{-1}$ for our *WISE*+SDSS+2MASS sources, and $\sim 40 \text{ mas yr}^{-1}$ for our SDSS+2MASS and *WISE*+SDSS sources, primarily due to shorter time baselines.

Comparison against the high proper motions stars from LSPM suggests good agreement for high proper motion stars in our catalog in all three subsamples (e.g., *WISE*+SDSS or SDSS+2MASS). For our subsamples, agreement with LSPM at the 2σ level was 98%, 97% and 96% for *WISE*+SDSS+2MASS, SDSS+2MASS, and *WISE*+SDSS, respectively (these all increase to 99% at

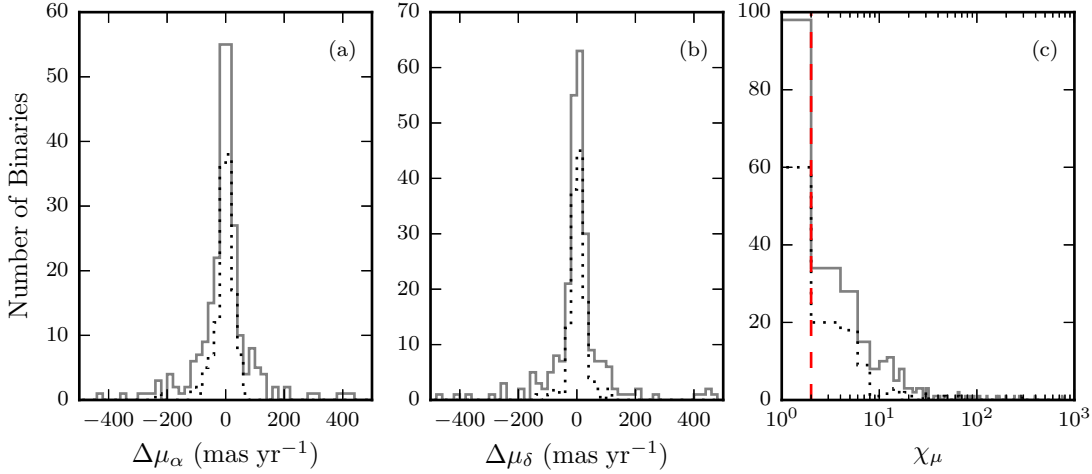


Figure 16. Distributions for proper motion residuals between the primary and secondary components for the stars matched between our MoVeRS catalog and SLoWPoKES-II. The solid line denotes all pairs matched, and the dotted line denotes only stars matched with all three epochs (i.e. *WISE*+SDSS+2MASS). Subplots (a) and (b) show the proper motion differences between the primary and secondary in α and δ , respectively. Both distributions are peaked at zero (dashed lines), showing good agreement between the proper motions. Subplot (c) shows equation (14), the quadrature sum of the weighted difference of both proper motion components. The red dotted line denotes a value of 2, the cutoff value for binaries to be include in the original SLoWPoKES catalog.

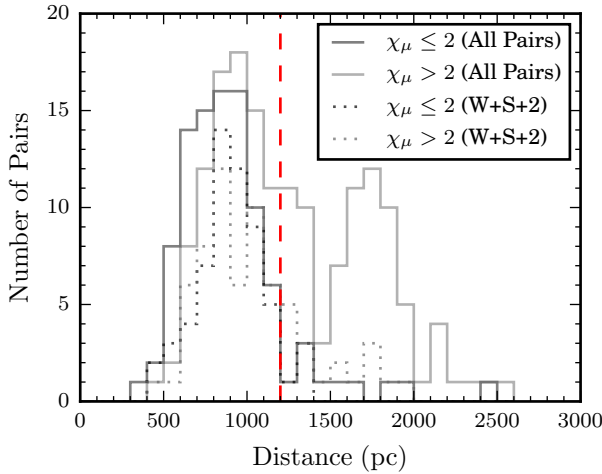


Figure 17. Average distance distributions for pairs from the SLoWPoKES-II catalog. Dark gray lines correspond to high-fidelity pairs ($\chi_\mu \leq 2$; equation 14), and light gray to low-fidelity ($\chi_\mu > 2$) pairs. Dotted lines correspond to all pairs found within MoVeRS, while solid lines correspond to only pairs where both components had three epochs (i.e. *WISE*+SDSS+2MASS). Pairs with an average distance > 1200 pc (dashed line) tend to have less similar proper motions (and hence lower fidelity) than closer pairs. The majority of pairs within SLoWPoKES-II have angular separations $< 8''$, so we expect many of the pairs to have high-reliability.

the 3σ level). We further compared our proper motions to SDSS+USNO-B measurements and the deeper proper motion catalog released by Munn et al. (2014). In both cases, our proper motion precision is strongly correlated with apparent magnitude and color, diminishing for bluer and fainter sources.

The utility of this catalog will be in the vast number of motion verified low-mass stars it contains, and its high reliability, specifically for the reddest and lowest-mass members of the catalog. We expect the red end of this catalog to surpass the limits of *Gaia*. Our catalog is available through SDSS CasJobs and VizieR.

The authors would first like to thank the anonymous referee for their extremely helpful comments which greatly improved the quality of this study. The authors would like to thank Ani Thankar for support running long queries on SDSS CasJobs on the behalf of this study, and for help uploading the catalog to CasJobs. The authors would also like to thank Benjamin Alan Weaver and Vandana Desai for their help with understanding the SDSS and 2MASS data, respectively. C.A.T. would like to thank Dylan Morgan, Julie Skinner, and Brandon Harrison for many helpful discussions. C.A.T. would like to acknowledge the Ford Foundation for financial support. A.A.W acknowledges funding from NSF grants AST-1109273 and AST-1255568. A.A.W. and C.A.T. also acknowledge the support of the Research Corporation for Science Advancement’s Cottrell Scholarship.

Funding for SDSS-III has been provided by the Alfred P. Sloan Foundation, the Participating Institutions, the National Science Foundation, and the U.S. Department of Energy Office of Science. The SDSS-III web site is <http://www.sdss3.org/>.

SDSS-III is managed by the Astrophysical Research Consortium for the Participating Institutions of the SDSS-III Collaboration including the University of Arizona, the Brazilian Participation Group, Brookhaven National Laboratory, Carnegie Mellon University, University of Florida, the French Participation Group, the German Participation Group, Harvard University, the Instituto de Astrofísica de Canarias, the Michigan State/Notre Dame/JINA Participation Group, Johns Hopkins University, Lawrence Berkeley National Laboratory, Max Planck Institute for Astrophysics, Max Planck Institute for Extraterrestrial Physics, New Mexico State University, New York University, Ohio State University, Pennsylvania State University, University of Portsmouth, Princeton University, the Spanish Participation Group, University of Tokyo, University of Utah, Vanderbilt University, University of Virginia, University of Washington, and Yale University.

This publication makes use of data products from the

Table 5
 $i - z$ Color Selection Criteria

$r - i$	$i - z$	# of Stars	Bin Size
0.200	0.367 ± 0.044	309784	0.01
0.205	0.367 ± 0.044	309784	0.01
0.215	0.379 ± 0.048	318938	0.01
...
2.010	2.685 ± 0.210	8	0.2
2.020	2.685 ± 0.210	8	0.2
2.030	2.685 ± 0.210	8	0.2

Note. — Table 5 is published in its entirety in the electronic edition of AJ, a portion is shown here for guidance regarding its form and content.

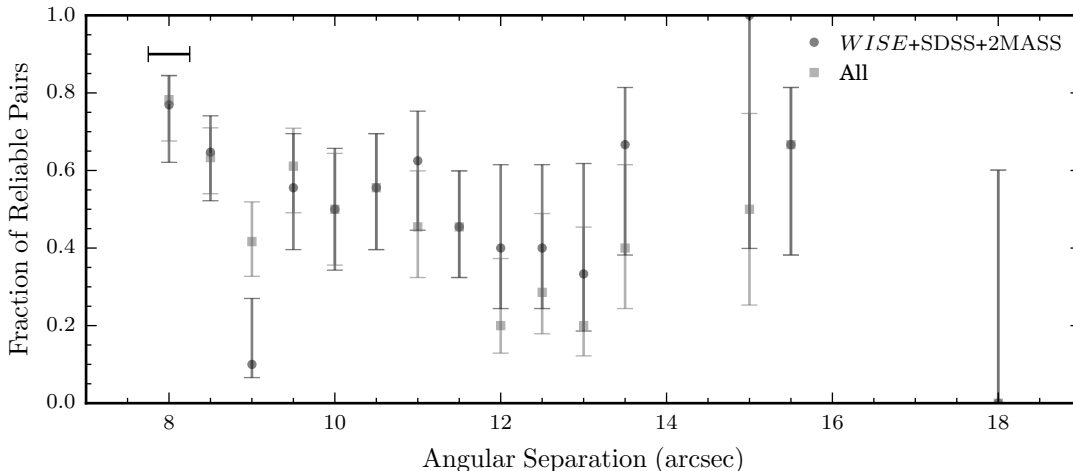


Figure 18. Reliability fraction of pairs (with reliable pairs defined as pairs with $\chi_\mu \leq 2$) as a function of angular separation between components. The bin size is shown in the top left corner. Only pairs with average distances ≤ 1200 pc were used. Reliability fractions were calculated for all matched pairs (light gray square), and pairs where both components had *WISE*+*SDSS*+*2MASS* measurements (dark gray circles). We did not find any reliable pairs with angular separations $> 15''$. Reliability increases for smaller angular separations, unfortunately we cannot probe the majority of the SLoWPoKES-II pairs, which have angular separations $< 8''$.

Two Micron All Sky Survey, which is a joint project of the University of Massachusetts and the Infrared Processing and Analysis Center/California Institute of Technology, funded by the National Aeronautics and Space Administration and the National Science Foundation.

This publication also makes use of data products from the *Wide-field Infrared Survey Explorer*, which is a joint project of the University of California, Los Angeles, and the Jet Propulsion Laboratory/California Institute of Technology, funded by the National Aeronautics and Space Administration.

This research made use of Astropy, a community-developed core Python package for Astronomy (Astropy

Collaboration et al. 2013). Figures in this work were created using the Python based graphics environment Matplotlib (Hunter 2007).

The authors are also pleased to acknowledge that much of the computational work reported on in this paper was performed on the Shared Computing Cluster which is administered by Boston University's Research Computing Services (www.bu.edu/tech/support/research/). In particular, C.A.T. would like to thank Paul Dalba and Yann Tambouret for helpful discussions regarding optimization of code and parallelization.

APPENDIX

A.1 COLOR SELECTION POLYGONS

Tables 5, 6, and 7 contain the color selection criteria we used to trace the stellar locus and select our initial sample.

A.2 QUERYING THE CATALOG

Our Motion Verified Red Stars (MoVeRS) catalog is available through SDSS CasJobs¹¹ and VizieR¹². To access our catalog through CasJobs, please refer to the documentation for accessing public tables. The following is an example SQL query for accessing our table within the DR10 context to return SDSS positions, *rizJHKW*1 photometry, proper motions, and proper motion errors for stars with: 1) total proper motions less than 500 mas yr^{-1} ; 2) total proper motion errors less than 20 mas yr^{-1} ; 3) $r - z > 2.5$; and 4) $18 < r < 21$:

¹¹ <http://skyserver.sdss.org/casjobs/>

¹² <http://vizier.u-strasbg.fr/viz-bin/VizieR>

Table 6
 $z - J$ Color Selection Criteria

$r - z$	$z - J$	# of Stars	Bin Size
0.500	1.030 ± 0.056	1384	0.01
0.505	1.030 ± 0.056	1384	0.01
0.515	1.033 ± 0.054	3861	0.01
...
4.900	2.076 ± 0.049	3	0.2
4.910	2.044 ± 0.024	2	0.2
4.920	2.044 ± 0.024	2	0.2

Note. — Table 6 is published in its entirety in the electronic edition of AJ, a portion is shown here for guidance regarding its form and content.

Table 7
 $z - W1$ Color Selection Criteria

$r - z$	$z - W1$	# of Stars	Bin Size
0.500	1.712 ± 0.096	4889	0.01
0.505	1.712 ± 0.096	4889	0.01
0.515	1.724 ± 0.096	13629	0.01
...
4.900	3.429 ± 0.082	3	0.2
4.910	3.373 ± 0.027	2	0.2
4.920	3.373 ± 0.027	2	0.2

Note. — Table 7 is published in its entirety in the electronic edition of AJ, a portion is shown here for guidance regarding its form and content.

SELECT

p.sdss_ra, p.sdss_dec, p.rmag, p.imag, p.zmag, p.jmag, p.hmag, p.kmag,
p.wlmpo, p.pmra, p.pmdec, p.pmra_toterr, p.pmdec_toterr

FROM public.LowMassPM.MoVERS p

WHERE

p.pmra * p.pmra + p.pmdec * p.pmdec < 500 * 500 AND
p.pmra_toterr * p.pmra_toterr + p.pmdec_toterr * p.pmdec_toterr < 20 * 20 AND
p.rmag - p.zmag > 2.5 AND
p.rmag BETWEEN 18 and 21

A.3 MOVERS CATALOG SCHEMA

Table 8
Catalog Schema

Field Name	Format	Units	Description
SDSS_OBJID	int64		SDSS DR8+ Object ID
SDSS_RA	float64	degrees	SDSS R.A.
SDSS_DEC	float64	degrees	SDSS Decl.
SDSS_RAERR	float32	degrees	SDSS R.A. error (in proper units, i.e. $\Delta\alpha \cos \delta$)
SDSS_DECERR	float32	degrees	SDSS Decl. error
SDSS_MJD	float32	days	SDSS r -band modified Julian date
UMAG	float32	mags	SDSS u -band PSF magnitude
GMAG	float32	mags	SDSS g -band PSF magnitude
RMAG	float32	mags	SDSS r -band PSF magnitude
IMAG	float32	mags	SDSS i -band PSF magnitude
ZMAG	float32	mags	SDSS z -band PSF magnitude
UMAG_ERR	float32	mags	SDSS u -band PSF magnitude error
GMAG_ERR	float32	mags	SDSS g -band PSF magnitude error
RMAG_ERR	float32	mags	SDSS r -band PSF magnitude error
IMAG_ERR	float32	mags	SDSS i -band PSF magnitude error
ZMAG_ERR	float32	mags	SDSS z -band PSF magnitude error
2MASS_RA	float32	degrees	2MASS R.A.
2MASS_DEC	float32	degrees	2MASS Decl.
2MASS_RAERR	float32	degrees	2MASS R.A. error (in proper units, i.e. $\Delta\alpha \cos \delta$)
2MASS_DECERR	float32	degrees	2MASS Decl. error
2MASS_MJD	float32	days	2MASS modified Julian date
2MASS_PH_QUAL	3 character string		2MASS photometric quality flag
2MASS_RD_FLG	3 character string		2MASS read flag
2MASS_BL_FLG	3 character string		2MASS blend flag

Table 8 — *Continued*

Field Name	Format	Units	Description
2MASS_CC.FLG	3 character string		2MASS contamination and confusion flag
2MASS_GAL.CONTAM	int32		2MASS extended source “contamination” flag
JMAG	float32	mags	2MASS <i>J</i> -band PSF magnitude
JMAG_ERR	float32	mags	2MASS <i>J</i> -band PSF corrected magnitude uncertainty
JMAG_ERRTOT	float32	mags	2MASS <i>J</i> -band PSF total magnitude uncertainty
JSNR	float32	mags	2MASS <i>J</i> -band SNR
HMAG	float32	mags	2MASS <i>H</i> -band PSF magnitude
HMAG_ERR	float32	mags	2MASS <i>H</i> -band PSF corrected magnitude uncertainty
HMAG_ERRTOT	float32	mags	2MASS <i>H</i> -band PSF total magnitude uncertainty
HSNR	float32	mags	2MASS <i>H</i> -band SNR
KMAG	float32	mags	2MASS <i>K_s</i> -band PSF magnitude
KMAG_ERR	float32	mags	2MASS <i>K_s</i> -band PSF corrected magnitude uncertainty
KMAG_ERRTOT	float32	mags	2MASS <i>K_s</i> -band PSF total magnitude uncertainty
KSNR	float32	mags	2MASS <i>K_s</i> -band SNR
J.PSFCHI	float32		2MASS <i>J</i> -band reduced χ^2 goodness-of-fit for the PSF
H.PSFCHI	float32		2MASS <i>H</i> -band reduced χ^2 goodness-of-fit for the PSF
K.PSFCHI	float32		2MASS <i>K_s</i> -band reduced χ^2 goodness-of-fit for the PSF
WISE_RA	float32	degrees	<i>WISE</i> R.A.
WISE_DEC	float32	degrees	<i>WISE</i> Decl.
WISE_RAERR	float32	degrees	<i>WISE</i> R.A. error (in proper units, i.e. $\Delta\alpha \cos \delta$)
WISE_DECERR	float32	degrees	<i>WISE</i> Decl. error
WISE_CC.FLG	4 character string		<i>WISE</i> contamination and confusion flag
WISE_EXT.FLG	int32		<i>WISE</i> extended source flag
WISE_VAR.FLG	4 character string		<i>WISE</i> variability flag
WISE_PH.QUAL	4 character string		<i>WISE</i> photometric quality flag
WISE_W1MJDMEAN	float32	days	<i>WISE</i> W1-band average modified Julian date
W1MJDSIG	float32	days	<i>WISE</i> MJD uncertainty ^a
W1MPRO	float64	mags	<i>WISE</i> W1-band PSF magnitude
W1SIGMPRO	float64	mags	<i>WISE</i> W1-band PSF magnitude uncertainty
W1SNR	float64		<i>WISE</i> W1-band SNR
W1RCHI2	float32		<i>WISE</i> reduced χ^2 goodness-of-fit for the PSF
NEAREST_NEIGHBOR	float32	arcsec	Distance to nearest SDSS primary object
NEAREST_RMAG	float32	mags	SDSS <i>r</i> -band PSF magnitude of nearest neighbor
NEAREST_IMAG	float32	mags	SDSS <i>i</i> -band PSF magnitude of nearest neighbor
NEAREST_ZMAG	float32	mags	SDSS <i>z</i> -band PSF magnitude of nearest neighbor
NEIGHBORS	int32		Number of SDSS primary objects within 15''
RR1	int32		Flag if there is an object within 8'' with $r_{\text{source}} - r_{\text{neighbor}} \geq -1$
RR2	int32		Flag if there is an object within 8'' with $r_{\text{source}} - r_{\text{neighbor}} \geq -2$
RR25	int32		Flag if there is an object within 8'' with $r_{\text{source}} - r_{\text{neighbor}} \geq -2.5$
RR3	int32		Flag if there is an object within 8'' with $r_{\text{source}} - r_{\text{neighbor}} \geq -3$
RR4	int32		Flag if there is an object within 8'' with $r_{\text{source}} - r_{\text{neighbor}} \geq -4$
RR5	int32		Flag if there is an object within 8'' with $r_{\text{source}} - r_{\text{neighbor}} \geq -5$
PMRA	float32	mas yr ⁻¹	Proper motion in R.A. (in proper units, i.e. $\mu_\alpha \cos \delta$)
PMDEC	float32	mas yr ⁻¹	Proper motion in Decl.
PMRA_M04	float32	mas yr ⁻¹	M04 Proper motion in R.A. (in proper units, i.e. $\mu_\alpha \cos \delta$)
PMDEC_M04	float32	mas yr ⁻¹	M04 Proper motion in Decl.
PMRA_INTERR	float32	mas yr ⁻¹	Intrinsic error in proper motion in R.A.
PMDEC_INTERR	float32	mas yr ⁻¹	Intrinsic error in proper motion in Decl.
PMRA_MEASERR	float32	mas yr ⁻¹	Measurement error in proper motion in R.A.
PMDEC_MEASERR	float32	mas yr ⁻¹	Measurement error in proper motion in Decl.
PMRA_FITERR	float32	mas yr ⁻¹	Fit error in proper motion in R.A.
PMDEC_FITERR	float32	mas yr ⁻¹	Fit error in proper motion in Decl.
PMRA_TOTERR	float32	mas yr ⁻¹	Combined error in proper motion in R.A.
PMDEC_TOTERR	float32	mas yr ⁻¹	Combined error in proper motion in Decl.
PMRAERR_M04	float32	mas yr ⁻¹	M04 error in proper motion in R.A.
PMDECERR_M04	float32	mas yr ⁻¹	M04 error in proper motion in Decl.
BASELINE	float32	years	Time baseline used to compute our proper motions
DBIT	3 character string		Detection bit identifying surveys used in computing proper motions ^b
RECOMP	int32		Flag indicating proper motions were recomputed (see Section 3.4.1)
USE	int32		Flag indicating which PM measurement to use ^c
MATCH_M04	int32		Number of SDSS objects within a 1'' radius matching the USNO-B object
SIGRA_M04	float32	mas	M04 RMS residual for the proper motion fit in R.A.
SIGDEC_M04	float32	mas	M04 RMS residual for the proper motion fit in Decl.
NFIT_M04	int32		Number of detections used in the M04 fit
O_M04	float32	mags	Recalibrated USNO-B O magnitude, recalibrated to SDSS <i>g</i>
J_M04	float32	mags	Recalibrated USNO-B J magnitude, recalibrated to SDSS <i>g</i>
WS_DIST	float32	arcsec	Total distance between <i>WISE</i> position and SDSS position ^d
S2_DIST	float32	arcsec	Total distance between SDSS position and 2MASS position ^d
W2_DIST	float32	arcsec	Total distance between <i>WISE</i> position and 2MASS position ^d

Table 8 — *Continued*

Field Name	Format	Units	Description
^a Defined as $.5 \times (W1MJD_{\text{MAX}} - W1MJD_{\text{MIN}})$. ^b ‘111’: <i>WISE</i> , SDSS, and 2MASS were used; ‘110’: SDSS and 2MASS were used; ‘011’: <i>WISE</i> and SDSS were used; ‘000’: SDSS+USNO-B measurement is available. ^c ‘1’: proper motions were measured here; ‘2’: proper motions are from M04; or ‘3’: both proper motions are available. ^d Total distance = $\sqrt{(\Delta\alpha)^2 \cos \delta_1 \cos \delta_2 + (\Delta\delta)^2}$.			
REFERENCES			
Abazajian, K. N., Adelman-McCarthy, J. K., Agüeros, M. A., et al. 2009, <i>ApJS</i> , 182, 543			Luyten, W. J. 1922, <i>Lick Observatory Bulletin</i> , 10, 135
Ahn, C. P., Alexandroff, R., Allende Prieto, C., et al. 2014, <i>ApJS</i> , 211, 17			Mainzer, A., Bauer, J., Grav, T., et al. 2011, <i>ApJ</i> , 731, 53
Astropy Collaboration, Robitaille, T. P., Tollerud, E. J., et al. 2013, <i>A&A</i> , 558, A33			Monet, D. 1996, in <i>Bulletin of the American Astronomical Society</i> , Vol. 28, Bulletin of the American Astronomical Society, 1282
Bochanski, J. J., Hawley, S. L., Covey, K. R., et al. 2010, <i>AJ</i> , 139, 2679			Monet, D., Canzian, B., & Henden, A. 1994, in <i>Bulletin of the American Astronomical Society</i> , Vol. 26, American Astronomical Society Meeting Abstracts, 1314
Bochanski, J. J., West, A. A., Hawley, S. L., & Covey, K. R. 2007, <i>AJ</i> , 133, 531			Monet, D. G. 1998, in <i>Bulletin of the American Astronomical Society</i> , Vol. 30, American Astronomical Society Meeting Abstracts, #120.03
Boggs, P. T., & Rogers, J. E. 1990, <i>Contemporary Mathematics</i> , 112, 183			Monet, D. G., Levine, S. E., Canzian, B., et al. 2003, <i>AJ</i> , 125, 984
Covey, K. R., Hawley, S. L., Bochanski, J. J., et al. 2008, <i>AJ</i> , 136, 1778			Munn, J. A., Monet, D. G., Levine, S. E., et al. 2004, <i>AJ</i> , 127, 3034
Davenport, J. R. A., Ivezić, Ž., Becker, A. C., et al. 2014, <i>MNRAS</i> , 440, 3430			—. 2008, <i>AJ</i> , 136, 895
Deacon, N. R., & Hambly, N. C. 2007, <i>A&A</i> , 468, 163			Munn, J. A., Harris, H. C., von Hippel, T., et al. 2014, <i>AJ</i> , 148, 132
Dhital, S., West, A. A., Stassun, K. G., & Bochanski, J. J. 2010, <i>AJ</i> , 139, 2566			Pâris, I., Petitjean, P., Aubourg, É., et al. 2014, <i>A&A</i> , 563, A54
Dhital, S., West, A. A., Stassun, K. G., et al. 2012, <i>AJ</i> , 143, 67			Perryman, M. A. C., Lindegren, L., Kovalevsky, J., et al. 1997, <i>A&A</i> , 323, L49
Dhital, S., West, A. A., Stassun, K. G., Schluns, K. J., & Massey, A. P. 2015, <i>AJ</i> , 150, 57			Perryman, M. A. C., de Boer, K. S., Gilmore, G., et al. 2001, <i>A&A</i> , 369, 339
Dong, R., Gunn, J., Knapp, G., Rockosi, C., & Blanton, M. 2011, <i>AJ</i> , 142, 116			Pier, J. R., Munn, J. A., Hindsley, R. B., et al. 2003, <i>AJ</i> , 125, 1559
Dressing, C. D., & Charbonneau, D. 2013, <i>ApJ</i> , 767, 95			Reid, I. N., Hawley, S. L., & Gizis, J. E. 1995, <i>AJ</i> , 110, 1838
—. 2015, <i>ApJ</i> , 807, 45			Röser, S., & Bastian, U. 1993, <i>Bulletin d’Information du Centre de Données Stellaires</i> , 42, 11
ESA, ed. 1997, <i>ESA Special Publication</i> , Vol. 1200, The HIPPARCOS and TYCHO catalogues. Astrometric and photometric star catalogues derived from the ESA HIPPARCOS Space Astrometry Mission			Röser, S., Demleitner, M., & Schilbach, E. 2010, <i>AJ</i> , 139, 2440
Faherty, J. K., Burgasser, A. J., Cruz, K. L., et al. 2009, <i>AJ</i> , 137, 1			Röser, S., Schilbach, E., Schwan, H., et al. 2008, <i>A&A</i> , 488, 401
Gould, A., & Kollmeier, J. A. 2004, <i>ApJS</i> , 152, 103			Savcheva, A. S., West, A. A., & Bochanski, J. J. 2014, <i>ApJ</i> , 794, 145
Grabowski, K., Carlin, J. L., Newberg, H. J., et al. 2015, <i>Research in Astronomy and Astrophysics</i> , 15, 849			Sesar, B., Ivezić, Ž., & Jurić, M. 2008, <i>ApJ</i> , 689, 1244
Hawley, S. L., Gizis, J. E., & Reid, I. N. 1996, <i>AJ</i> , 112, 2799			Skrutskie, M. F., Cutri, R. M., Stiening, R., et al. 2006, <i>AJ</i> , 131, 1163
Hawley, S. L., Covey, K. R., Knapp, G. R., et al. 2002, <i>AJ</i> , 123, 3409			West, A. A., Morgan, D. P., Bochanski, J. J., et al. 2011, <i>AJ</i> , 141, 97
Høg, E., Fabricius, C., Makarov, V. V., et al. 2000, <i>A&A</i> , 355, L27			Wright, E. L., Eisenhardt, P. R. M., Mainzer, A. K., et al. 2010, <i>AJ</i> , 140, 1868
Hunter, J. D. 2007, <i>Computing in Science and Engineering</i> , 9, 90			Wu, Z.-Y., Ma, J., & Zhou, X. 2011, <i>PASP</i> , 123, 1313
Ivezić, Ž., Beers, T. C., & Jurić, M. 2012, <i>ARA&A</i> , 50, 251			York, D. G., Adelman, J., Anderson, Jr., J. E., et al. 2000, <i>AJ</i> , 120, 1579
Ivezić, Z., Tyson, J. A., Abel, B., et al. 2008, <i>ArXiv e-prints</i>			Zacharias, N., Finch, C. T., Girard, T. M., et al. 2013, <i>AJ</i> , 145, 44
Jones, D. O., West, A. A., & Foster, J. B. 2011, <i>AJ</i> , 142, 44			Zacharias, N., & Gaume, R. 2011, in <i>Journées Systèmes de Référence Spatio-temporels 2010</i> , ed. N. Capitaine, 95–100
Kilic, M., Munn, J. A., Harris, H. C., et al. 2006, <i>AJ</i> , 131, 582			Zacharias, N., Urban, S. E., Zacharias, M. I., et al. 2000, <i>AJ</i> , 120, 2131
Laughlin, G., Bodenheimer, P., & Adams, F. C. 1997, <i>ApJ</i> , 482, 420			Zacharias, N., Finch, C., Subasavage, J., et al. 2015, <i>ArXiv e-prints</i>
Lépine, S., & Shara, M. M. 2005, <i>AJ</i> , 129, 1483			Zhang, Z. H., Pokorný, R. S., Jones, H. R. A., et al. 2009, <i>A&A</i> , 497, 619
López-Corredoira, M. 2014, <i>A&A</i> , 563, A128			
Lupton, R., Gunn, J. E., Ivezić, Z., Knapp, G. R., & Kent, S. 2001, in <i>Astronomical Society of the Pacific Conference Series</i> , Vol. 238, <i>Astronomical Data Analysis Software and Systems X</i> , ed. F. R. Harnden, Jr., F. A. Primini, & H. E. Payne, 269			